Mitochondrial profiling reveals dynamic, sex- and age-specific mitochondrial phenotypes in human immune cell subtypes

Shannon Rausser[1], Caroline Trumpff[1], Marlon A McGill[1], Alex Junker[1], Wei Wang[2], Siu-hong Ho[2], Anika Mitchell[1], Kalpita R Karan[1], Catherine Monk[1,5,6], Suzanne C. Segerstrom[3], Rebecca G. Reed[4], Martin Picard[1,6,7]

[1] Department of Psychiatry, Division of Behavioral Medicine, Columbia University Irving Medical Center, New York, NY 10032, USA

[2] Columbia Center for Translational Immunology, Columbia University Irving Medical Center, New York, NY 10032, USA

[3] Department of Psychology, University of Kentucky, Lexington, KY, 40506, USA

[4] Department of Psychology, University of Pittsburgh, Pittsburgh, PA, 15260, USA

[5] Department of Neurology, Merritt Center, Columbia University Irving Medical Center, New York, NY 10032, USA

[6] Department of Obstetrics & Gynecology, Columbia University Irving Medical Center, New York, NY 10032, USA

[7] New York State Psychiatric Institute, New York, NY 10032, USA

Correspondence: martin.picard@columbia.edu

Abstract

How mitochondria functionally differ between immune cell subtypes, between the sexes, across ages, and whether they dynamically change over time has not been characterized. Here we deploy a high-throughput mitochondrial phenotyping platform to define cell-type specific mitochondrial features in circulating immune cell subtypes. In women and men spanning four decades of life, we find that mitochondrial content, mitochondrial DNA copy number (mtDNAcn), and respiratory chain enzymatic activities vary by up to 3.5-fold between neutrophils, monocytes, B and T lymphocyte subtypes. Within individuals, mitochondrial content and mtDNAcn, and to a lesser degree respiratory chain function, are strongly correlated with each other across immune cell types, suggesting their systemic harmonization. Moreover, repeated weekly measurements of mitochondrial features in the same individual reveal remarkable variation in mitochondrial content and respiratory chain function over time. This suggests that immune cell mitochondria exhibit dynamic state properties, which we find to be partially correlated with circulating biomarkers. We also define multivariate mitochondrial phenotypes – *mitotypes* – that distinguish lymphoid from myeloid cell types, naïve-to-memory lymphocyte states, and moderately differ between women and men. Finally, we compare mitochondrial features of purified cell subtypes to peripheral blood mononuclear cells (PBMCs) and determine the influence of contaminating platelets and of variable cell type composition. Our results invite caution in using cell type mixtures to infer person-level mitochondrial behavior. Together, these findings identify dynamic cell-type specific variation in mitochondrial biology among circulating leukocytes and provide foundational knowledge to develop interpretable blood-based assays of mitochondrial health.

Keywords: mitochondria; leukocytes; sexual dimorphism; aging; natural variation

Introduction

Mitochondria are unique organelles that contain their own genome and functionality based on the cell type they inhabit (Pagliarini et al., 2008; Picard et al., 2012a). For the immune system, mitochondria are essential to energy production and intracellular signaling. Among both myeloid and lymphoid lineages, mitochondrial metabolism guides the acquisition of specialized cellular characteristics during differentiation (Pearce et al., 2013). Notably, the activation, proliferation, and differentiation of both monocytes (Nomura et al., 2016) and T cells (Michalek et al., 2011) into specific effector cells require distinct metabolic profiles and cannot proceed without the proper metabolic states. For example, quiescent naïve and memory T lymphocytes derive energy through mitochondrial oxidative phosphorylation (OXPHOS) involving the respiratory chain (RC) (Jones et al., 2019), whereas T lymphocytes rapidly transition to anabolic metabolism and glycolysis as the main source of energy during activation (Brand, 1985; Ron-Harel et al., 2019). Thus, based on rodent and *in vitro* stimulation studies, different circulating immune cell subtypes that co-exist within a person should exhibit stable differences in both mitochondrial content and function, but this has not yet been fully defined in humans.

Certain facets of immune functioning also vary with age and sex. Sex differences in immune phenotypes are at least in part mediated by sex hormones, including testosterone and estrogens, which influence both the innate and adaptive arms of immunity (Furman et al., 2014). Sex hormones are known to influence the expression and enzymatic activities of RC complexes in other tissues including muscles, liver, and the brain (Cavalcanti-de-Albuquerque et al., 2014; Khalifa et al., 2017; Torres et al., 2018). Previous studies have also reported sex differences in the proportions of circulating immune cells, specifically within the innate immune system where activated natural killer (NK) cells are more abundant in men compared to women (Patin et al., 2018). In contrast, women have more of the mucosal-associated invariant T (MAIT) cells across all ages, suggestive of early hormonal influence on immune cell development (Patin et al., 2018). In relation to aging, increasing age is associated with continuous stimulation of innate and adaptive immune cells, leading to immune dysregulation and increased risk of chronic disease (Meier et al., 2020). In relation to cell type distribution, aging is also associated with decreasing abundance of circulating naïve T cells, particularly $CD8^+$ T cells, and increasing abundance of memory lymphocyte subtypes (Patin et al., 2018). But to what extent sex and age influence mitochondrial content and function within these different immune cell populations remains unknown.

Given the accumulating evidence for a role of mitochondrial (dys)function as a major determinant of disease risk and aging (Jang et al., 2018; Picard et al., 2016; Wallace, 2015) and as a mediator of psycho-biological processes (Picard et al., 2019), there is an increasing need for methods to map mitochondrial content and function in humans. Technically, we need to determine whether mitochondrial profiling in conveniently-isolated mixed cell populations such as peripheral blood mononuclear cells (PBMCs) is equivalent to and/or reflects specific cell subtypes, or whether PBMC measurements are confounded by biological factors such as i) cell type composition and ii) platelet contamination. Behavioral factors and diurnal cycles mobilize specific immune cell types from lymphoid organs into circulation and can therefore substantially alter mixed leukocyte composition (Dhabhar et al., 1994). In relation to mitochondria, the major immune cell subtypes also have different respiratory properties and mitochondrial RC protein abundance (Chacko et al., 2013), suggesting, along with animal studies referenced above, that variation in cell type abundance may bias mitochondrial features in mixed cells. Moreover, commonly used Ficoll-isolated PBMCs are contaminated with (sticky) platelets, which themselves contain mitochondria and mtDNA but no nuclear genome to use as reference for mtDNA copy number (mtDNAcn) measurements (Hurtado-Roca et al., 2016), adding another potential source of bias to mitochondrial studies in PBMCs or other undefined cell mixtures. To enable scalable translational mitochondrial research, there is therefore a need to develop biologically valid measures of mitochondrial health in specific immune cells and to quantify the influence of cell type abundance and platelet contamination on specific features of mitochondrial behavior.

Mitochondria are multifunctional organelles and various features of mitochondrial content (the mass of mitochondria per cell) and function (energy production capacity) undergo dynamic recalibrations in response to chronic stress exposure (for a review see (Picard and McEwen, 2018)). Well-defined mitochondrial recalibrations to stress (Picard and McEwen, 2018) and exercise (Gan et al., 2018) suggest that mitochondrial features of content and function could exhibit natural variation over time. Moreover, to quantify energy production capacity on a per-mitochondrion basis, individual biochemical and molecular markers of mitochondrial content and RC activity must be interpreted in tandem. These can be mathematically integrated into composite multivariate indices such as the bioenergetic health index (BHI) (Chacko et al., 2016) and the mitochondrial health index (MHI) (Picard et al., 2018). However, little is known about the nature and magnitude of inter-individual differences in mitochondrial phenotypes within specific immunologically-defined immune cell subtypes. An equally significant gap in knowledge relates to the natural dynamic variation in mitochondrial behavior: are leukocyte mitochondrial content

and RC function stable trait-like properties, or are they state-like features that vary over time, possibly in response to metabolic or endocrine mediators?

To address these questions, here we isolate immunologically-defined immune cell subtypes by flow cytometry, in parallel with PBMCs, and deploy a high-throughput mitochondrial phenotyping platform to define cell-specific profiles of mitochondrial content, mtDNAcn, and RC activity in relation to age, sex, and key biomarkers. To establish the natural within-person variation in mitochondrial features, we extend this approach in a repeated-measures design within the same individual across 9 time points. We also develop multivariate mitochondrial phenotypes, or *mitotypes,* that exhibit stable differences between immune cell lineages among both the cohort and repeat participant. Finally, we experimentally determine the influence of platelet contamination on mitochondrial features in PBMCs. Collectively, these data define unique cell-specific mitochondrial features in circulating human leukocytes, providing a foundation to apply immune mitochondrial phenotyping in clinical and epidemiological studies.

Results

Cell subtype distributions by age and sex

Our goal was to perform mitochondrial profiling on molecularly-defined subtypes of immune cell populations. Twenty one participants (11 women, 10 men) distributed across 4 decades of life (ages 20-59, 4-8 participants per decade across both sexes) were recruited, and ~100ml of blood was collected; total leukocytes were then labeled with two cell surface marker cocktails, counted and isolated by fluorescence-activated cell sorting (FACS, see *Methods* for details), and processed on our mitochondrial phenotyping platform (Picard et al., 2018) (Figure 1a). In parallel, a complete blood count (CBC) for the major leukocyte populations in whole blood was performed, in addition to standard blood chemistry and a selected metabolic and hormonal panel (Figure 1b).

We first quantified the abundance of specific cell subtypes based on cell surface marker combinations listed in Figure 1c (see Supplemental Figures 1 and 2 for the gating strategy and Supplemental Table 1 for subtype functions), including innate (neutrophils, NK cells, and monocytes) and adaptive T and B lymphocytes. We further distinguished $CD4^+$ and $CD8^+$ T cells by their naïve and memory states, including central (CM) and effector memory (EM), as well as terminally differentiated effector memory cells re-expressing CD45RA (TEMRA) subtypes. Evaluating the abundance of each cell subtype among participants, we found that compared to

women, men had on average 35-44% more NK cells and monocytes, but 66% less $CD4^+$ naïve T cells (Figure 1d). These differences were characterized by moderate to large standardized effect sizes (Hedges' g=0.71-0.93), confirming as previously established (Patin et al., 2018) that the composition of circulating immune cells differ between women and men. We also note that between individual participants, the circulating proportions of various cell subtypes (e.g., B and T lymphocytes, monocytes) varied by up to an order of magnitude (i.e., 10-fold) (Figure 1e).

In relation to age, as expected (Patin et al., 2018) $CD8^+$ naïve T cells abundance was lower in older individuals ($p<0.01$) such that, compared to young adults in their 20's, middle-aged individuals in their 50's had on average ~63% fewer $CD8^+$ naïve T cells (Figure 1f). In contrast, $CD4^+$ EM and $CD8^+$ CM abundance tended to increase with age (positive correlation, r=0.31 for both), an overall picture consistent with immunological aging (Nikolich-Žugich, 2014; Patin et al., 2018).

We then repeated this analysis with CBC-derived cell proportions and found that compared to women, men had on average 28% more monocytes (Supplemental Figure 3), consistent with our FACS results. Conversely, compared to men, women had on average 20% more platelets. Platelet abundance also tended to decrease with age, a point discussed later.

Next, we built on these results to define mitochondrial phenotypes for different cell subtypes. Our analysis focused on two broad aspects of mitochondrial biology: i) *mitochondrial content*, measured by citrate synthase (CS) activity, a Kreb's cycle enzyme used as a marker of mitochondrial volume density (Larsen et al., 2012), and mtDNAcn, reflecting the number of mtDNA copies per cell; and ii) *RC function* measured by complex I (CI), complex II (CII) and complex IV (CIV) enzymatic activities, which reflect the capacity for electron transport and respiratory capacity and serve here as a proxy for maximal oxidative phosphorylation (OXPHOS) capacity (Figure 1a). To obtain sufficient numbers of cells for mitochondrial phenotyping, we selected the 6 most abundant cell subtypes for each individual and isolated 5 million cells for each sample. Because memory subtypes were relatively rare, central and effector memory (CM and EM) subtypes were pooled for $CD4^+$ and/or $CD8^+$ (CM-EM). This generated a total of 340 biological samples, including 136 biological replicates, yielding 204 individual person-to-cell-type combinations used for mitochondrial phenotyping.

Purified cell subtypes differ in their mitochondrial content and RC function

CS activity was highest in monocytes and B cells, and lowest in $CD4^+$ naïve T cells, with other cell types exhibiting intermediate levels (Figure 2a). Regarding mitochondrial genome

content, B cells had the highest mtDNAcn with an average 451 copies per cell compared to neutrophils and NK cells, which contained only an average of 128 (g=5.94, p<0.0001) and 205 copies (g=3.84, p<0.0001) per cell, respectively (Figure 2b). Naïve and memory $CD4^+$ and $CD8^+$ T lymphocytes had intermediate mtDNAcn levels of ~300 copies per cell, with the exception of $CD8^+$ naïve cells (average of 427 copies per cell). Between cell types, we note that CS activity and mtDNAcn differed by up to 3.52-fold, providing initial evidence of strong effect size segregation of cell type-specific mitochondrial phenotypes among both innate and adaptive cell lineages.

In relation to RC function, monocytes had the highest Complexes I, II, and IV activities. Consistent with their low mtDNAcn, neutrophils also had the lowest activities across complexes, whereas naïve and memory subtypes of T and B lymphocytes presented intermediate RC enzyme activities (Figure 2c-e).

To understand the proportion of shared variance between mitochondrial content features (CS and mtDNA) and between RC complex enzymatic activities, we quantified their inter-correlations among all cell types. Interestingly, CS and mtDNAcn were only weakly correlated with each other, and in some cases were negatively correlated. For RC complexes CI, CII, and CIV, which physically interact and whose function is synergistic within the inner mitochondrial membrane, correlations tended to be positive, as expected (Figure 2f). However, some of these correlations were weak, and some were either not correlated or even negatively correlated within specific cell types. These relatively weak and absent inter-correlations between mitochondrial features in some cell types reveal that rather than being redundant measures, each metric provides relatively independent information about immune cell mitochondrial biology.

Mitochondrial health index (MHI) among cell subtypes

To further define how RC function relates to mitochondrial content, we integrated content and function features into a single metric known as the mitochondrial health index (MHI) (Picard et al., 2018). By adding the three mean-centered features of RC function together as a numerator (CI+CII+CIV), and dividing this by the combination of content features (CS+mtDNAcn), we obtained an index reflecting *RC capacity on a per-mitochondrion basis* (Figure 3a). Of all cell types, monocytes had the highest MHI, which was 72% higher than B cells (g=3.78, p<0.0001) which presented the lowest MHI (Figure 3b). On average, memory T cell subtypes exhibited a 6-18% higher MHI relative to their naïve precursors ($CD4^+$: g=0.40, p=0.32; $CD8^+$: g=1.02, p=0.019),

consistent with the notion that naïve and activated immune cells have different bioenergetic requirements (Nicoli et al., 2018; van der Windt et al., 2013).

Mitochondrial features exhibit differential co-regulation across immune cell subtypes

We next asked to what extent mitochondrial markers are correlated among different cell subtypes in the same person. For example, does the individual with the highest mtDNAcn in B cells also have the highest mtDNAcn in other cell types? Could having high mtDNAcn or low CIV activity constitute coherent properties of an individual that are expressed ubiquitously across cell types, or are these private properties to each cell subtype?

To assess the extent to which mitochondrial features are correlated across cell subtypes (co-regulation) we used Spearman correlation matrices, which revealed a general positive association (Figure 3c). Within a person, CS activity was moderately co-regulated across cell subtypes (average correlation $r_{z'}$=0.63), albeit with some exceptions (i.e., cell pairs that were less correlated than average, such as $CD4^+$ CM-EM T cells & B cells). Similarly, mtDNAcn was generally positively correlated between cell types (average correlation $r_{z'}$=0.53). We note that compared to CM-EM subtypes, naïve T lymphocyte mtDNAcn values tended to be more strongly correlated with other cell subtypes (r=0.32-0.93), indicating that co-regulation of mtDNAcn varies by cell type. In comparison, RC enzymes showed markedly lower inter-correlations across cell types (Figure 3d) and some cell types showed no correlation with other cell types, revealing a substantially lower degree of co-regulation among RC components than in mitochondrial content features. However, there was moderate evidence of co-regulation across cell types for MHI (average $r_{z'}$=0.37).

These findings show that while immune cells exhibit markedly different mitochondrial content and RC activities (see Figure 2), there is evidence for a person-level factor. On the other hand, the absence of correlation among several cell types, particularly for RC enzymatic activities, suggests that the biology of immune cell subtypes could be relatively independently determined by cell-autonomous factors (e.g., stimulation of specific cell subtypes or subpopulations). This provides a rationale for performing cell-type specific studies when examining the influence of external exposures and person-level factors on immune cells' mitochondrial bioenergetics, including the influence of sex and age.

Mitochondrial content and RC function differ between women and men

In each cell subtype, we then systematically compared CS activity, mtDNAcn, RC activity, and MHI features between women and men (Figure 4a-f). Across all cell subtypes examined,

compared to men, women had higher CS activity (range: 4-29%, g=0.20-1.52, Figure 4a) and higher CII activity (range:1-10%, g=0.03-0.56, Figure 4d). The consistency of this finding across all cell types suggests that these differences are stable, sexually dimorphic characteristics. Women also showed 29% higher CS activity in $CD8^+$ memory subsets and 26% higher CI activity in monocytes, differences characterized by strong effect sizes (g=1.52 and 1.35, respectively).

Compared to women, men exhibited higher mtDNAcn in monocytes and neutrophils (range: 5-12%, g=0.37-0.73, Figure 4b), higher CI activity in neutrophils and NK cells (range: 9-13%, g=0.26-0.64, Figure 4c), and higher CIV activity in B cells (20%, g=0.53, Figure 4e). Cells exhibiting the largest degree of sexual dimorphism on the integrated MHI were neutrophils (17% higher in women, g=0.52) and B cells (12% higher in men, g=0.73) (Figure 4f). These data reveal cell subtype-specific (and possibly lineage-specific) sex differences in human immune cell mitochondria.

Age influences mitochondrial content and RC function

We then quantified the association between the same mitochondrial features and age (correlations) for each cell subtype. With increasing age, CS activity was relatively unaffected except in neutrophils, where it decreased ~7% per decade (r=-0.63, p=0.031) (Figure 4g). In comparison, mtDNAcn increased with increasing age among all cell subtypes except $CD8^+$ naïve T cells which was, interestingly, the cell subtype exhibiting the strongest age-related decline in abundance in circulation. $CD4^+$ naïve T cells and monocytes showed the largest age-related change in mtDNAcn, marked by a ~10% increase in the number of mitochondrial genomes per cell per decade of life (r=0.54 for both, p=0.022 and 0.023 respectively, Figure 4h). Thus, in purified cell subtype preparations (free of platelets and other confounds), aging is associated with a consistent increase in leukocyte mtDNAcn.

For RC function, we mostly observed an equal number of cell subtypes with either positive or negative correlations with age, with the exception of CII (Figures 4i-k). CII activity was positively correlated with age across all cell types, except for monocytes and NK cells where it was independent from age. In contrast, CI and CIV activities were only weakly associated with age, highlighting again differential regulation of RC components. Of all cell types, $CD8^+$ CM-EM T cells showed the most consistent positive associations for all RC activities and age, notably for CII where the enzymatic activity per cell increased ~21% per decade (r=0.85, p=0.0004). $CD4^+$ naïve T cells were the only cell type showing a consistent, albeit modest, increase of both mitochondrial content and function with age (range:1-10% increase per decade, r=0.08-0.54, Supplemental

Figure 4). Similarly, MHI correlated positively with age in $CD8^+$ CM-EM T cells, indicating that energy production capacity on a per-mitochondrion basis tends to increase with age in this cell type (r=0.56, p=0.052), possibly related to the acquisition or maintenance of memory characteristics. In contrast, MHI tended to correlate negatively with age in monocytes (r=-0.35, p=0.15) (Figure 4l). Overall, these data demonstrate that age-related changes in CS activity, mtDNAcn, and RC function are largely cell-type specific.

Cell subtype distributions exhibit natural week-to-week variation

Whether and how much mitochondrial content or function change over time in various cells and tissues is not well defined, and to our knowledge has not been examined in circulating human immune cells. Here we repeated the same blood collection, cell sorting, and downstream mitochondrial enzymatic and molecular procedures described above to perform weekly mitochondrial profiling on a healthy 34-year-old Caucasian man (author M.P.) over 9 weeks (Figure 5a). To preclude external influences on cell subtype distributions and mitochondrial function, each blood draw occurred at the same time of day (9am), on the same day of the week, after a standardized breakfast, and comparable physical activity. The 6 most abundant cell subtypes for this individual included neutrophils, NK cells, monocytes, naïve and CM-EM subtypes of $CD4^+$ T cells, and naïve $CD8^+$ T cells. The resulting samples were processed on the mitochondrial phenotyping platform in parallel with the cohort samples, ensuring that results across the cohort and repeat participant are directly comparable.

We first quantified the circulating proportions (% of total leukocytes by FACS) of 12 cell types to establish how much the abundance of each cell subtype naturally varies within a person (Supplemental Figure 5). Cell type distribution is known to exhibit natural diurnal variation (Ackermann et al., 2012; Dhabhar et al., 1994) and can be altered with stress exposure in rats and humans (Beis et al., 2018; Dhabhar et al., 2012). The cell subtype with the least week-to-week variation in abundance was $CD8^+$ EM (root mean square of successive differences (rMSSD)=0.22, coefficient of variation (C.V.)=19.5%), which varied between 6.3% (week 2, highest) to 3.3% of total cells (week 9, lowest). Thus, even the least variable cell type can decrease in proportion by approximately half in the span of a few weeks. In contrast, other subtypes such as $CD4^+$ TEMRA (min=0.02% to max=0.62%) and neutrophils (min=3.9% to max=31.8%) varied week-to-week by as much as an order of magnitude (i.e., 10-fold), similar to between-person differences observed in the cohort (see Figure 1e and Supplemental Table 2). Antibody-producing B cells, which had the highest mtDNAcn, varied by up to 1.1-fold (min=0.86% to max=1.8%). Together, these time-course results illustrate the dynamic remodeling of circulating

leukocyte populations within a single person. In addition, these data suggest that cell mixtures (e.g. PBMCs) are likely to be confounded by unequal abundance of different cell types on different occasions of sampling, a point addressed later.

Mitochondrial content, mtDNAcn and RC activity exhibit natural week-to-week variation

We quantified mitochondrial features reflecting content and RC function in each available cell type across the 9 time points. The first observation was that the robust cell type differences reported above in our cohort were conserved in the repeat participant. Monocytes had the highest RC activity, neutrophils the lowest, and $CD4^+$ and $CD8^+$ T lymphocytes showed intermediate activities. Similarly, the cell subtype with the highest mtDNAcn was $CD8^+$ naïve T cells (average across 9 weeks=400 copies/cell, 427 in the cohort) and neutrophils exhibited the lowest mtDNAcn in both the repeat participant and the cohort (average=123 copies/cell, 128 in the cohort).

Within specific cell subtypes, we found that all mitochondrial metrics exhibited substantial variation over time. Within the same person, different cell types showed week-to-week variation ranging from 7.3 to 21.9% for CS activity, 4.1 to 18.3% for mtDNAcn, 8.4 to 37.5% for CI, 4.1 to 15.3% for CII, and 15.2 to 64.4% for CIV (Figure 5b-f). Similarly, MHI in each subtype varied by 8.3 to 20.6%, with the naïve subsets of $CD4^+$ and $CD8^+$ T lymphocytes exhibiting the largest week-to-week changes (rMSSD=0.28 and 0.22, respectively) (Figure 5g). In most cases, the observed variation was significantly greater than the established technical variation in our assays (see Supplemental Table 3), providing confidence that these changes in mitochondrial content and function over time reflect robust biological changes.

To put this natural biological variation in perspective, we directly compared the inter- and intra- individual variation of mitochondrial metrics. Specifically, we asked: relative to differences observed among a heterogeneous cohort of women and men spanning 4 decades of life, how much do the same metrics naturally vary within a single person. Remarkably, for several mitochondrial metrics, the 9-week range and natural variation within the same person was similar to the between-person differences among our 21-participant cohort. Figure 5h provides a side-by-side comparison of the cohort and repeat participant CS activity on the same scale. The C.V. of CS in monocytes was 17.0% for the cohort and 20.2% in the repeat participant. Similarly, in $CD4^+$ naïve T cells, the dynamic range for CS activity among both the cohort and repeat participant was similar. Supplemental Figure 6 shows side-by-side comparisons of between- and within-person variation for mtDNAcn, CI, CII, CIV, and MHI. The similar degree of variation in the cohort and repeat participant indicates that dynamic variation is a generalizable property across

all mitochondrial features examined. This also suggests that future research designs should incorporate repeated measures of specific mitochondrial metrics to ensure the reliability of mitochondrial content and function features.

Next, we assessed the co-regulation of mitochondrial content and RC activity across cell subtypes within the same person over time. Despite the small sample of timepoints for these comparisons, similar to our cohort findings, CS and mtDNAcn were most highly correlated across cell types (average $r_{z'}$=0.55-0.70) (Figure 5i-j). Again, RC activities were only moderately correlated, indicating partial co-regulation of mitochondrial energetics across some cell subtypes. Of the RC complexes, CI was the most consistent across cell subtypes (average $r_{z'}$=0.39), whereas CIV showed the least co-regulation (average $r_{z'}$=0.06) including several negative correlations (Figure 5j). For example, when CIV activity for this individual increased in monocytes, CIV activity tended to similarly increase in $CD4^+$ CM-EM T cells (r=0.71, p=0.088), but tended to decrease in $CD8^+$ naïve T cells (r=-0.68, p=0.11). Altogether, these within-person data were consistent with our cohort findings (between individuals) indicating partial co-regulation of mitochondrial features across cell subtypes, including some negative associations that remain unexplained.

Compiling all cell subtype pairs for each mitochondrial feature, we then systematically evaluated the level of agreement between the cohort and the repeat participant. In other words, we asked if two cell subtypes (e.g., $CD4^+$ and $CD8^+$ naïve) are highly correlated for a given mitochondrial feature (e.g., CS) among the cohort, do these cell subtypes also show high correlation within a single person over time? The presence of most datapoints in the upper right quadrants of Figure 5k supports the general conclusion that mitochondrial features - particularly CS and mtDNAcn - are generally co-regulated across cell types within both the cohort and a single person over time. However, the level of agreement between the cohort and repeat participant was generally weak to moderate (r=0.08-0.35, absolute values), possibly pointing to person-level differences in how mitochondrial behavior among different cell types relate to each other.

Because these and previous results somewhat differed by mitochondrial feature, and because each feature reflects a slightly different aspect of mitochondrial biology, we then mathematically combined multiple variables to investigate cell subtype-specific mitochondrial phenotypes.

Mitotypes differ between immune cell subtypes

As in other complex biological systems, the function and behavior of mitochondria require synergy among multiple features. For that reason, the functional characteristics of mitochondria may be defined by multivariate approaches examining the inter-relations of multiple mitochondrial features. This logic is similar to body mass index (BMI), which puts height and weight into a BMI ratio that is more easily interpretable and meaningful than either height or weight features alone. For example, in human mitochondrial tissues, the ratio of CIV and CII activities (also known as COX/SDH ratio) is used in diagnoses of mitochondrial dysfunction, whereas alone either CIV or CII activity is less easily interpretable (Picard et al., 2012b). Thus, integrating primary features of mitochondrial content, genome abundance, and RC function produces integrated mitochondrial phenotypes, or *mitotypes*, which reflect the functional specialization of mitochondria among different cell subtypes, or among dynamic cellular states.

Similar to BMI, the mitotypes analyzed (listed and defined in Supplemental Figure 7) are computed from the ratio of two or more mitochondrial features. Each mitotype can be visualized as a scatterplot with two variables of interest as the x and y axes (Figure 6a). In the example in Figure 6a, the hypothetical cell type A has a higher value for feature 2 relative to feature 1 (Mitotype A), while cell type B has a higher value for feature 1 relative to feature 2 (Mitotype B). Note that if both features increase or decrease following the same proportions, the ratio is the same and follows a diagonal on the mitotype graph, reflecting an invariant mitotype. Thus, similar to BMI, changes in mitotypes are reflected by perpendicular movement relative to the diagonal in the mitotype space.

Given that leukocyte subtypes differ widely in their bioenergetic properties, we asked in our cohort (n=21 individuals) if different cell subtypes have different mitotypes. The first mitotype examined puts in relation mtDNA copies per cell (mtDNAcn) relative to mitochondrial content per cell (CS activity), creating a mitotype (mtDNAcn/CS) that reflects *mtDNA density per mitochondrion* (Figure 6b). Alone, this mtDNA density mitotype provided remarkable separation of cell subtypes. Neutrophils and NK cells were low on both metrics, B cells were high on both metrics, monocytes had the lowest mtDNA density, whereas $CD8^+$ naïve T cells exhibited the highest mtDNA density of all cell subtypes tested. Figures 6c-e illustrate other mitotypes including i) CII activity per unit of mitochondrial genome (CII/mtDNAcn), as well as more complex combinations of variables such as ii) CI activity per unit of mtDNA (CI/mtDNAcn ratio on y axis) in relation to mtDNA density (mtDNAcn/CS activity on x axis), and iii) CI activity per mitochondrial content (CI/CS, y) in relation to mtDNA density (mtDNAcn/CS, x). We understand these mitotype combinations to reflect the well-known principles of mitochondrial functional specialization (Calvo

et al., 2016; Picard et al., 2012a) and to represent individual mitochondrial “personality types" tailored to subserve specific bioenergetic and biosynthetic requirements within immune cell subtypes.

This mitotype-based analysis of mitochondrial characteristics revealed two main points. First, cells of the innate and adaptive immune subdivisions contain mitochondria that differ not only quantitatively in their individual metrics of mitochondrial content and RC activity, but that exhibit marked qualitative differences. This is illustrated by the distinct clustering of neutrophils, monocytes and NK cells (innate) within similar mitotype spaces, and the clustering of all lymphocyte subtypes together in different spaces. Compared to cells of the innate immune compartment, lymphocytes (adaptive) had higher mtDNAcn and lower respiratory chain activity. A second insight from this analysis is that compared to naïve subsets of $CD4^+$ and $CD8^+$ T cells, which themselves have relatively distinct mitotypes (e.g., CII/mtDNAcn, Figure 6c), both memory $CD4^+$ and $CD8^+$ subtypes converged to similar mitotype spaces. Functionally, this naïve-to-memory mitotype transition is well known to involve a metabolic shift including changes in spare respiratory capacity, mitochondrial content, glucose and fatty acid uptake (Nicoli et al., 2018; van der Windt et al., 2012). The mitotype analysis showed that compared to naïve cell subtypes, memory subtypes exhibit 26-29% lower mtDNA density per mitochondrion, but an 8-23% increase in RC activity per mitochondrion in $CD4^+$ T cells, although not in $CD8^+$ T cells (Figure 6f).

Stability of mitotypes

Next, we examined how stable these cell-type specific mitotypes were in the independent repeat participant dataset. We plotted matching cell types for the cohort and for the repeat participant on the same mitotype plots. As for the cohort, cell types belonging to the innate and adaptive immune divisions similarly clustered together, and naïve and memory subtypes differences were also validated at the within-person level (Figure 6g-i), demonstrating the conserved nature of immune cell mitotypes.

To examine the biological stability of mitotypes across individuals, we determined the effect sizes between cell subtypes for selected mitotypes in our cohort, and then compared these to the magnitude of the differences between the cohort and the repeat participant for specific cell subtypes (Figure 6j). First, consistent with the results for individual mitochondrial features (see Figure 2), the effect sizes comparing mitotypes between cell subtypes ranged from moderate to very large. For example, mitotype differences between monocytes and $CD8^+$ naïve T lymphocytes had effect sizes ranging from g=2.5 to 3.5. Neutrophils and NK cells, which were among the most

similar cell types on most mitotype plots, had Hedges' g values ranging from 0.2 (small) to 1.2 (very large), reflecting some considerable mitotype differences even among these cell types. In comparison, inter-individual variation (cohort n=21 vs repeat n=9) across different mitotypes was over an order of magnitude smaller, with pooled effects sizes being on average 12.5-fold smaller than cell type differences. Overall, these data across both the mixed cohort of women and men, and within-person repeated-measures, reveal that immune cell subtypes have distinct and robust mitotypes consistent with their divergent bioenergetic requirements.

Evidence for a sex and age bias in mitotypes

We next sought to systematically examine if mitotypes differ between women and men. Mitotypes were organized into five categories of indices based upon their features, yielding a total of 16 mathematically-distinct mitotypes (see Supplemental Figure 7). For each mitotype, we quantified the magnitude of the difference between women and men by the effect size (g), ranked all mitotype x cell subtype combinations (16 mitotypes x 9 cell subtypes), and analyzed the distribution of these indices by sex. The majority of mitotypes reflecting mitochondrial RC activities per CS activity were higher in men ($p<0.0001$, Chi-square), while RC activity per mtDNA density ($p<0.001$) and RC activity per genome in relation to mtDNA density mitotypes ($p<0.01$) were predominantly higher in women (Figure 7a). The magnitude of sex differences ranged from 17% higher in men (CI/CS in $CD4^+$ CM-EM T cells, g=1.14) to 38% higher in women (CII/mtDNA density in neutrophils, g=1.37) (Figure 7b). The direction of sex differences for all mitotypes (e.g. higher in women or in men) with effect sizes is illustrated in Figure 7c**.** Compared to purified cell subtypes, the magnitude of sex differences in the PBMCs cell mixture appeared blunted. The average effect size across all mitotypes was 0.31 (small) in $CD4^+$ naïve T cells, compared to monocytes where the average effect size was 0.71 (medium).

Using the same approach, we then systematically quantified the relationship between mitotypes and age. Mitotypes reflecting RC activity per CS activity were predominantly positively correlated with age ($p=0.046$), while RC activities per genome in relation to mtDNA density mitotypes were generally negatively correlated with age ($p=0.012$) (Figure 7d). This finding is consistent with the overall age-related increase in mtDNAcn across cell subtypes, and could indicate a general decrease in the RC output per unit of mitochondrial genome with aging in immune cells. The strength of these correlations ranged from $r=-0.67$ to 0.75 (Figure 7e). The correlations of individual mitotypes with age for each cell subtype are shown in Figure 7f.

Overall, these findings reveal consistent patterns of differences in immune cell mitotypes between women and men, and to a lesser extent with aging. Importantly, these data also indicate

that the observed differences vary considerably by cell subtype. Whereas innate immune cells exhibited the strongest sex differences, B cells exhibited the largest age-related mitotype changes.

Associations of blood biomarkers with subtype-specific mitochondrial features

To explore the source of inter-individual differences and within-person dynamics over time, we asked to what extent blood biomarkers were correlated with subtype-specific mitochondrial features. To do so, we examined sex hormones, inflammatory markers, metabolic markers, and standard clinical blood biochemistry in relation to subtype-specific mitochondrial features (Figure 8a). Because mitochondrial features in specific cell types, as well as blood biomarkers, were both associated with sex and age, we examined sex- and age- adjusted partial correlations. At the cohort level, associations between blood biomarkers and cell subtype mitochondrial phenotypes were relatively weak (Figure 8b). These results indicate that circulating neuroendocrine, metabolic and inflammatory factors are unlikely to explain a large fraction of the variance in inter-individual differences in mitochondrial biology, pointing instead to behavioral, genetic and other influences as the source of inter-individual variation.

We then examined this question at the within-person level where week-to-week variation is independent of constitutional and genetic influences, and where behavior (e.g., levels of physical activity, sleep patterns, etc.) is more stable relative to the behavioral differences between women and men of different ages. Compared to the cohort, the strength of associations between biomarkers and mitochondrial metrics across cell types was on average 1.7-fold larger in the repeat participant (average absolute values, $r_{z'}$=0.39 for the repeat participant vs 0.23 for the cohort) (Figure 8c). Another notable finding was the difference in the correlation patterns between different cell subtypes, which again suggest that different mitotypes, or the cells that host them, may exhibit different sensitivities to circulating neuroendocrine, metabolic, or biochemical factors.

Notable patterns of associations between circulating biomarkers and mitochondrial features emerged at the within-person level. For instance, lipid levels including triglycerides, total cholesterol, and low- and high-density lipoproteins (LDL, HDL) were positively correlated with CS activity and mtDNAcn, with the largest effect sizes observed among innate immune cells: neutrophils, NK cells, and monocytes (Figure 8c, red area on the heatmap). In these cells, lipid levels accounted on average for 53% of the variance (r^2) in CS activity and 47% in mtDNAcn. We note that some of these estimates are likely overestimated due to the small number of repeated measures. Nevertheless, compared to CS and mtDNAcn, these associations were less consistent

for RC enzyme activities and MHI. We speculate that the positive association of lipid levels and mitochondrial content features in innate immune cells could reflect the action of lipid signaling pathways well known to stimulate mitochondrial biogenesis in other tissue types (Iershov et al., 2019; Lindquist et al., 2018; Picard et al., 2012b; Turner et al., 2007).

We next sought to examine potential divergences in the associations among the cohort compared to the repeat participant. It is established that different individuals show remarkably different baseline levels of both mitochondrial features and blood biochemistry measures (e.g., some people have higher blood cholesterol than others). Moreover, our data shows that within a person, there is also extensive physiological variation in mitochondrial features and in blood biochemistry over time. Therefore, we reasoned that *even* if each participant in our cohort was to exhibit a strong positive correlation between LDL and CS activity over time, sampling each person on a single randomly selected occasion would not reveal this positive correlation at the group level. As an illustration of this point, in the repeat participant we found an association between lipids and mitochondrial content (LDL and neutrophil CS activity, $r=0.90$, $p<0.01$) that was not observed in the cohort, where each datapoint represents a single time point for a given person (panel 1 of Figure 8d). The lack of association in the cohort was apparent despite a substantially larger dynamic range in LDL in the cohort relative to the repeat participant (43-180 vs 105-134 mg/dL, respectively). On the other hand, between-person comparisons in the cohort may also reveal apparent associations that are not observed within any of the individuals among the cohort or the repeat participant (Figure 8d, panels 3 and 4).

Altogether, although not definitive, the divergence in the correlation strengths and patterns between the cohort and repeat participant (Figure 8e) highlight the potential value of repeated-measures designs to examine the influence of humoral factors on mitochondrial biology in immune cells.

Association of cell subtypes abundance and enzymatic activities with total PBMCs

Compared to isolating purified cell subtypes, cell mixtures such as PBMCs are more easily collected and require less blood volume to obtain a sufficient number of cells for downstream analyses. As a result, PBMCs have been the preferred material of choice in leukocyte studies examining environmental influences on mitochondria (Dixon et al., 2019; Karabatsiakis et al., 2014; Weiss et al., 2015). However, in light of our results revealing i) large variation in the abundance of circulating cell types, both between- and within-person, and ii) large effect size

differences between cell subtypes across all mitochondrial features, it is reasonable to assume that cell mixtures are likely to be confounded by cell type distribution.

Therefore, we analyzed the same mitochondrial features in both FACS-purified cell subtypes and PBMCs of the same person, and first asked to what extent PBMCs reflect mitochondrial content and function of isolated cell subtypes. If PBMCs were comprised solely of those individual cell types, mitochondrial activities normalized on a per-cell basis in PBMCs could only be as high as the highest cell subtype it contains (e.g., B cells), and as low as the lowest (e.g., neutrophils). Curiously, we found that PBMCs had up to 2.9-fold higher levels of CS, CI, and CII activity per cell than any of the individual cell subtypes measured (see Figure 2), casting initial doubt on the validity of mitochondrial activity measures in PBMCs. This discrepancy could be attributable to contamination of PBMCs with platelets, which contain mitochondria but no nucleus used for normalization per cell (see section below). PBMCs also had an unexpectedly high MHI, similar to NK cells and monocytes, and generally higher than naïve lymphocytes (Figure 3b).

Starting with individual mitochondrial features, we examined if the co-regulation among features observed in individual cell subtypes is also present in PBMCs. Consistent with previous work in PBMCs (Picard et al., 2018), CS activity and mtDNAcn were positively correlated with each other, as were RC complexes CI, CII, and CIV (Figure 2f). In fact, of all cell types, PBMCs consistently showed the highest inter-correlations among mitochondrial features.

We also asked to what extent the influence of sex and age on mitochondrial phenotypes observed in purified cell subtypes can be detected in total PBMCs. Our data revealed a markedly smaller association between sex and PBMCs mitochondrial activities (g=0.10-0.40) relative to isolated cell subtypes (Figure 4a-f). Likewise, PBMCs mitochondrial content and function features did not significantly correlate with age (r=0.008-0.15, absolute values) (Figure 4g-l). These results are in stark contrast to individual cell subtypes, revealing that PBMCs either do not show age- and sex-related associations that exist among some of its constituent cells, or that these associations are strongly blunted.

When evaluating the stability of PBMCs mitochondrial content and function over time in the repeat participant, we found that PBMCs CS activity, mtDNAcn, and RC activity varied by 9.8-61.9%, similar to the variation observed in isolated subtypes (C.V. range: 4.1-64.4%) (Figure 5a-g). For mtDNAcn, CI, and CII activities, PBMCs showed either similar or higher week-to-week variation than neutrophils, the cell subtype with the greatest dynamic variation on these

mitochondrial features (despite the absence of neutrophils in PBMCs). Thus, PBMCs exhibit at least an equivalent degree of dynamic variation over time as individual cell subtypes.

For co-regulation analyses across individual cell subtypes, among our cohort, mitochondrial features in PBMCs were moderately to not correlated with individual cell subtypes (Figure 3c, Supplemental Figure 8a). In the repeated-measures participant however, the associations between the cell subtypes and PBMCs mitochondrial features tended to be stronger (Figure 5i, Supplemental Figure 8b-c). In particular, CS activity and mtDNAcn were highly correlated between PBMCs and innate immune cells. In contrast, the associations of mitochondrial features in PBMCs with naïve and memory lymphocytes were more modest, even though lymphocytes are expected to constitute the largest cellular fraction in PBMCs. Thus, PBMCs exhibit substantial dynamic changes among several mitochondrial features that appear relatively independent from mitochondrial features in lymphocyte populations, but coupled to innate immune cells.

We then compared PBMCs and other cell subtypes based on the same multivariate mitotype spaces described above. As Figure 6b-e shows, PBMCs generally exhibit a similar mitotype (diagonal line from the origin of the plot) as innate immune cell subtypes (monocytes, NK cells, and neutrophils), appearing relatively distinct from lymphocyte subpopulations. In relation to mitotype sensitivities to sex and age differences, similar to analyses on single metrics, PBMCs showed among the weakest associations with either variable (Figure 7c and f). Thus, even if specific cell subtypes reveal sex- and age-related differences, PBMCs provide modest between-person sensitivity to detect these associations.

PBMCs are a biologically distinct entity from individual cell subtypes

To understand the origin of the divergences identified above between PBMCs and individual cell subtypes, we determined how much potential influence the abundance of various circulating immune cell subtypes has on individual mitochondrial metrics in PBMCs. The null hypothesis here is that cell type abundances (e.g., having more or fewer B cells in circulation) does not influence PBMCs mitochondrial features. We first estimated the proportion of variance in PBMCs mitochondrial features attributable to cell type abundance measured by flow cytometry (Figure 9a). Contrary to the null hypothesis, the proportion of circulating B cells accounted for 27% of the variance in PBMCs mtDNAcn, and for 32-61% of the variance in CS, CI, and CII activities. These findings were consistent with the fact that B cells had the highest mtDNAcn of all cell subtypes, and the fact that individuals varied substantially in B cell proportions (range: <0.01-

15.3%) (Supplemental Table 2). The proportion of other cell types accounted for more modest portions (<14%) of the variance in PBMCs, although we note that higher abundance of memory cells tended to be negatively associated with PBMCs activities.

Interestingly, the pattern of associations was markedly different when we analyzed within-person changes in the repeat participant (Figure 9b). Contrary to the cohort, B cell abundance did not predict PBMCs mtDNAcn or enzymatic activities at the within-person level, possibly because of the limited range in circulating B cell abundance (0.95% week-to-week range in the repeat participant vs 15% range in the cohort). Within-person, the abundance of $CD4^+$ naïve T cells was positively correlated with PBMCs mtDNAcn, CS and CI activity, similar in direction to what was observed at the group level. But on average, compared to the cohort, the associations between the proportion of cell subtypes and PBMCs mitochondrial features tended to be stronger and more negative, as noted by the abundance of negative correlations in Figure 9c. In particular, at the time points when the participant had higher circulating levels of EM and TEMRA $CD4^+$ and $CD8^+$ lymphocytes, most mitochondrial features were considerably lower in PBMCs. Interestingly, the associations were in the opposite direction (positive) for CM subtypes, suggesting a potentially meaningful functional distinction between central and effector memory subtypes in relation to PBMCs.

We repeated this analysis with CBC-derived cell proportions to examine the association of broad leukocyte groups with mitochondrial features in PBMCs. In the cohort, the abundance of eosinophils and neutrophils was positively correlated with most PBMCs mitochondrial content and activity features (Supplemental Figure 8d-e). Because PBMCs do not contain granulocytes, it appears more likely that these correlations reflect the independent effect of a humoral factor on cell mobilization and PBMCs mitochondria. At the within-person level, compared to the cohort, again associations between CBC-derived cell proportions and PBMCs mitochondrial features tended to be weaker and more negative (Supplemental Figure 8f).

Together, these data show that mitochondrial features assessed in PBMCs in part reflect the proportions of some but not all circulating cell subtypes, objectively documenting cell type distribution as a confounding factor in the measurements of mitochondrial function in PBMCs. Moreover, our cohort vs within-person comparison suggests that these confounding factors may vary based on the study design (within- vs between-person), calling for future within-person studies with repeated mitochondrial measures.

Platelets influence PBMCs mitochondrial phenotypes

Platelets contain mitochondria and mtDNA, but no nucleus. Because cell-based normalization procedures rely on the presence of the nuclear genome, platelets are essentially invisible to cell-based normalization procedures and therefore inflate mitochondrial activities on a per-cell basis. Moreover, platelets are naturally adherent and easily form platelet-leukocyte aggregates (Butler et al., 2007), such that they typically "contaminate" leukocyte preparations and inflate mtDNAcn measurements (Hurtado-Roca et al., 2016) (Figure 10a). Therefore, in order to partly resolve the origin of the discrepancies between isolated cell subtypes and PBMCs notes above, we sought to quantify the contribution of platelets to total mitochondrial content and activity features in PBMCs.

We first asked if the abundance of platelets from the CBC data in the cohort changes with age. In our cohort, we found that platelet count decreased by 6% for each decade of life (Figure 10b), declining by an average of 24% between the ages of 20 and 60. The loss of platelets with age, in women and men, is consistent with two large epidemiological studies of >40,000 individuals each (Biino et al., 2013; Zhang et al., 2015), although the effect sizes vary by cohort (Figure 10c). In our data, we also found that platelet count tended to be positively correlated with mtDNAcn, CS and RC activities in PBMCs (r=0.031-0.38) (Figure 10d), suggesting that PBMCs preparations from individuals with more circulating platelets may contain more contaminating platelets. Therefore, the age-related loss of platelets and of the mtDNA contained within them could account for the previously reported age-related decline in mtDNAcn from studies using either whole blood (Mengel-From et al., 2014; Verhoeven et al., 2018) (which includes all platelets) or PBMCs (Zhang et al., 2017) (which includes only contaminating platelets). In contrast, as noted above (see Figure 2), our analysis in purified cell subtypes reveal an age-related *increase* in mtDNAcn among most cell types. Therefore, platelet contamination could influence PBMCs mitochondrial features and explain the discrepancies with purified cell types, including why PBMCs have higher CS activity values than any of its constituent cells.

To directly test this hypothesis, we ran a separate experiment to assess the influence of platelets on total PBMCs mitochondrial features (Figure 10e). This consisted of isolating PBMCs using standard methods, which included two standard low speed "platelet depletion" steps (see *Methods* for details). A portion of the obtained PBMCs platelets were then actively immunodepleted using anti-CD61-tagged magnetic beads. Three fractions were ultimately processed for mitochondrial phenotyping and compared: i) total PBMCs, ii) platelet-depleted PBMCs, and iii) platelet-enriched eluate from the depletion procedure. As expected, platelet depletion decreased mtDNAcn, CS, and RC activities, indicating that contaminating platelets

exaggerated specific mitochondrial features by 9-22%, with exception to CIV (Figure 10f). Moreover, the platelet-enriched eluate showed 23-100% higher mitochondrial activities relative to total PBMCs, providing further evidence that platelet depletion was effective and that platelets inflated estimates of mitochondrial abundance and RC activity in standard PBMCs.

Interestingly, the composite MHI was not affected by the platelet depletion procedure, suggesting that this multivariate index of respiratory chain capacity on a per-mitochondrion basis may be more robust to platelet contamination than individual features. Overall, these data demonstrate platelet-contamination even in carefully prepared PBMCs, and show that the magnitude of platelet contamination represents a potential source of noise for PBMCs-based mitochondrial studies.

Discussion

Mapping the naturally occurring bioenergetic differences among various tissues and cell types is critical to further our understanding of the role of mitochondria in human health and disease. Here we have used the immune system as a model to examine this question, isolating and phenotyping multiple immune cell subtypes among a diverse cohort of women and men, and in repeated weekly measures in the same participant. Using a high-throughput mitochondrial phenotyping platform including five primary mitochondrial features and a derived MHI, we find large functional differences between immune cell subtypes in mitochondrial features reflecting both mitochondrial content and respiratory chain function. These mitochondrial features also vary moderately by age and sex. In addition, we uncover large week-to-week within-person variation in both cell subtype proportions and mitochondrial behavior. We also introduce multivariate mitotypes, which constitute a first step towards identifying stable cell-type specific bioenergetic profiles. Together with the direct comparison of these features in PBMCs cell mixtures, these data in specific leukocyte populations provide foundational knowledge on mitochondrial phenotypes in human immune cells, their sensitivity to inter-individual variables such as age and sex, and highlights the value of repeated-measures designs to examine the mechanisms of dynamic mitochondrial variation in humans.

There has been emerging interest in determining what dictates the natural variability of immune cell subtype distributions, which are in large part driven by intrinsic genetic, environmental, and behavioral factors in humans (Patin et al., 2018). In relation to the metabolic properties of specific immune cells subtypes, most data is derived from rodents or from human

leukocytes often activated *in vitro*, which clearly demonstrates that immune cells exhibit specific metabolic requirements depending on their state (Artyomov and Van den Bossche, 2020; Makowski et al., 2020; Pearce et al., 2013). Our analysis first confirmed the influence of sex and age on the proportions of circulating innate and adaptive cells, likely reflecting the effect of genetic and environmental factors throughout life. In relation to metabolic profiling, our ability to deploy mitochondrial phenotyping to hundreds of samples with a throughput and sensitivity not previously possible revealed consistent cell type differences in multiple mitochondrial features, reflecting mitochondrial content and respiratory chain function. By any standard, the magnitude of the observed differences, for example in mtDNAcn (up to 3.5-fold differences between cell subtypes, g=5.94), is very large. The combination of a heterogenous cohort and a repeat participant design also allowed us to further quantify the stability of these cell subtype differences over time. Examining the molecular basis for these cell type differences could represent a unique opportunity to delineate the mechanisms responsible for controlling mitochondrial mass, mtDNAcn, and/or functional specialization within accessible human cells. In relation to mitochondrial genome regulation, the age-related increase in mtDNAcn among most cell types deserves particular attention.

Defining the temporal aspects of human immunometabolism is a major frontier that, when overcome, will transform our knowledge of fundamental immune and mitochondrial biology, and allow for the rational design of therapeutic approaches (Artyomov and Van den Bossche, 2020). A primary finding of this work is the natural within-person variation of mitochondrial features, providing insight into the temporal dynamics of immunometabolism in specific human cell subtype populations. The existence of large inter-individual differences in mitochondrial features between the immunologically-defined cell subpopulations noted above naturally called for repeated-measures conducted with the same degree of biological specificity. As such, cell sorting removes the potential confound of week-to-week changes in cell type distributions, an inherent confounding variable in PBMCs, and therefore adds confidence in the robustness of such temporal mitochondrial variation. This within-person analysis revealed that mitochondrial features within immune cells exhibit state-like properties that vary by >20-30% week-to-week. These findings warrant for future studies investigating the factors that drive these changes. We had previously observed that up to 12% of the inter-individual variation in MHI was attributable to positive mood (ratings of positive experiences such as excited, hopeful, inspired, love) the night prior (Picard et al., 2018), suggesting that psychosocial factors could in part contribute to a substantial portion of the dynamic variation in leukocyte mitochondrial function. However, this study was performed in

PBMCs and although it included repeated measures of psychosocial factors to establish directionality of the psycho-mitochondrial association, it only included one measurement time point for MHI. Additional work is therefore needed to disentangle the independent contributions of behavioral, psychosocial, nutritional, and other factors on mitochondrial features in humans. Importantly, we note that our results demonstrate mitochondrial changes taking place within less than one week. Therefore, establishing the exact temporal dynamics of leukocyte mitochondrial variations will require repeated assessments with even greater temporal resolution.

A particularly striking observation is that the dynamic changes in cell subtype-specific mitochondrial features within a person can, in some cell types, be of similar magnitude to the biological variation observed among a heterogenous reference cohort of 21 individuals composed of women and men spanning four decades of life. Thus, a single measure of mitochondrial function may not accurately reflect a given person's average mitochondrial functional capacity. To account for naturally occurring within-person variation in mitochondrial biology, as for other biological markers with high intra-person variation (e.g., cortisol (Segerstrom et al., 2017)), our result highlights the importance for future research of repeated-measures designs to capture statistically stable inter-individual differences.

Our mitotype approach, while exploratory, also provided further insight on the mitochondrial functional specialization among circulating human immune cell subtypes. Most notably, the innate and adaptive subdivisions, as well as the metabolic transition from naïve T lymphocytes to memory states, both harbored distinct mitotypes. Here also, we found mitotypes of specific cell subtypes to be relatively conserved between our heterogenous cohort and repeat participant. Thus, the mitotype approach may help to achieve an understanding of both quantitative and qualitative differences in mitochondrial phenotypes. Moreover, the mitotype analysis revealed potentially generalizable sex- and age-related differences in mitochondrial features.

In relation to sex differences, animal studies have consistently identified sexually dimorphic mitochondrial features, including greater mitochondrial content in females (reviewed in (Ventura-Clapier et al., 2019)). Likewise, a study in humans showed that PBMCs from women have greater CS activity, and greater CI and CII-mediated respiration (Silaidos et al., 2018). Consistent with previous findings, our data show similar changes in enzymatic activities for most, but not all, cell types, highlighting that the magnitude of sex differences is likely cell-type specific.

Therefore, the use of methods offering a sufficient level of biological specificity appear warranted to reproducibly and accurately quantify these sex differences in different contexts.

In relation to age, previous studies in whole blood (Mengel-From et al., 2014; Verhoeven et al., 2018), PBMCs (Zhang et al., 2017), and muscle tissue (Hebert et al., 2015; Short et al., 2005) have consistently reported an age-related decline in mtDNAcn. However, these studies, particularly those in blood, are confounded by the existence of cell mixtures and platelet contamination. In a study of 672 adults where these confounds were measured and used in statistical adjustments, accounting for cell type distribution and platelet count eliminated previous associations between mtDNAcn and age (Moore et al., 2018). Our data, like previous studies (Hurtado-Roca et al., 2016), demonstrates how platelets inflate mtDNAcn, as well as other mitochondrial features. Integration of data across two population-based studies and our cohort show that platelet number consistently decreases with age, which could account for the apparent decline in blood or PBMCs mtDNAcn when sampling individuals across the lifespan – older individuals have fewer platelets, and therefore appear to have less mtDNA copies per cell, even if cellular mtDNAcn is actually unchanged. In fact, we find that cellular mtDNAcn in immunologically-defined and FACS-isolated leukocyte subtypes exhibit a positive association with age – increasing by as much as 10% per decade. Given the accumulation of mtDNA mutations and deletions with age (e.g., (Ye et al., 2014; Zhang et al., 2017)), and that mtDNA defects can trigger the compensatory upregulation of mtDNAcn to counteract the loss of intact mitochondria associated with age (Giordano et al., 2014; Yu-Wai-Man et al., 2010), the observed positive correlation of mtDNAcn with age could reflect compensatory upregulation of mtDNA replication in response to bioenergetic dysfunction. The only cell type examined that did not exhibit an age-related positive association with mtDNAcn are $CD8^+$ naïve T cells, which, interestingly, is the only cell type whose abundance in circulation significantly declines with advancing age. The basis for this correlation requires further investigation.

Because PBMCs are widely used across fields, mostly due to their ease of collection, we wanted to examine whether they would reflect or mask observations in specific cell subtypes. In many cases, robust associations in specific cell subtypes were either not observed or blunted in PBMCs. For example, there was no correlation between age and PBMCs MHI either in this study or previously (Karan et al., 2020), but correlations were present in purified cell subtypes. Interestingly, the mitotype analysis revealed similar mitotypes between total PBMCs and cells of the innate subdivision, namely neutrophils, NK cells, and monocytes (often aligned along the same mitotype diagonal space on mitotype plots). In the mitotype plots, if PBMCs were composed

uniquely of a mixture of lymphocytes and monocytes, the natural expectation is that PBMCs would lie somewhere between the specific subsets that compose it. Instead, PBMCs, occupy an entirely different and unexpected mitotype space, indicating the presence of a contaminating factor. The platelet depletion experiment leaves little doubt that platelet contamination skews the measurements of several mitochondrial features, with some features being apparently more affected than others. Although we cannot entirely rule out potential contamination of individual cell types with residual platelets, the FACS labeling, wash, and sorting procedures must produce the purest sample with the highest degree of biological specificity.

This study presents limitations that should be noted. First, we acknowledge the relatively small sample size of the cohort, and the exhaustive repeated-measures in only one participant. We included an equal representation of women and men in the cohort, but grouping by sex further reduced the sample size for subgroup analyses and may have led to difficulty identifying statistically significant results. Additionally, because our mitochondrial phenotyping platform currently requires ~5 million cells per sample, we only collected the six most abundant cell subtypes from each participant, which in some instances reduced the final sample size for different cell subtypes. However, we provide evidence for the variable proportions of cell subtypes from person-to-person, which determined which cell subtypes were collected from each participant. In order to accommodate the minimum cell number per sample, central and effector memory subtypes were grouped, although they may exhibit differences not examined here. Furthermore, we recognize that additional cell surface markers may be useful to identify cell populations not included here (e.g. activated or adaptive lymphocyte subtypes). Finally, we did not test participants for CMV status, which may have provided additional insight into the age-related effects on immune cell subtypes.

Altogether, these results define mitochondrial phenotypes among circulating immune cell subpopulations in humans and provide evidence that these features are in part influenced by sex and age. The repeated-measures of mitochondrial content and function in the same person also provide insight into the natural within-person variation of cell subtypes and dynamic mitochondrial profiles from week-to-week. Additionally, our mitotype approach identifies conserved multivariate phenotypic distinctions between lymphoid and myeloid cells, and naïve-to-memory lymphocyte states. Finally, our correlative PBMCs results in the cohort and repeat participant, together with the effects of active platelet-depletion, invite caution in the use and interpretation of mitochondrial measurements from cell mixtures such as PBMCs. Further research into the dynamic, state-like

mitochondrial properties of immune cell subtypes is necessary to understand both the causes of these variations, and their implications on the immune system and on health outcomes.

Methods

Participants

The study was approved by New York State Psychiatric Institute (Protocol #7618). All participants provided written informed consent. Healthy adults between 20 and 60 years willing to donate blood were eligible for inclusion. Exclusion criteria included severe cognitive deficit, symptoms of flu or other seasonal infection four weeks preceding the visit, involvement in other clinical trials, malignancy or other clinical condition, and diagnosis of mitochondrial disease. Participants were recruited via flyers posted in the Columbia University Irving Medical Center (CUIMC) community. Participants completed a short demographic questionnaire, anthropometric measurements (weight, height, heart rate, and blood pressure), and a blood draw. The main study cohort included twenty-one individuals (11 women, 10 men), mean age 36 ±11 (SD, range: 23-57), were recruited. The ethnic breakdown of our sample was: 2 African Americans, 7 Asians, and 12 Caucasians. All blood draws took place in the morning between 9-10am. Additionally, repeated weekly measures were collected across 9 weeks from one healthy Caucasian man (author M.P., 34 years old) to assess within-person variability in mitochondrial measures and immune cell type distribution. To standardize and minimize the influence of nutritional and behavioral factors in the repeat participant, repeated measures were collected at the same time (9:00am), on the same day of the week (Fridays), after a standardized breakfast (chocolate crepe), ~30-60 minutes after a regular bicycle commute to study site.

Blood Collection

*A total o*f 100 ml of blood was drawn from the antecubital vein for each participant and included one EDTA tube (Cat# BD367841, 2 ml) for complete blood count (CBC), two SST coated tubes (Cat#BD367986, 5 ml) for hormonal measures and blood biochemistry in serum, and 11 Acid Dextrose A (ACD-A) tubes (Cat# BD364606, 8.5 ml) for leukocyte isolation and mitochondrial analyses, in order of collection. All tubes were gently inverted 10-12 times immediately after draw to ensure proper mixing. The EDTA and SST tubes for hematological and blood biochemistry were processed by the Center for Advanced Laboratory Medicine (CALM) Lab, and the ACD-A tubes were further processed for cell isolation.

PBMCs and leukocyte isolation

Ficoll 1077 and 1119 (Sigma), Hanks Balanced Salt Sodium (HBSS) without phenol red, calcium and magnesium (Life Technologies, Cat# 14175103) supplemented with 2% BSA (Sigma, Cat# A9576) (HBSS/BSA), HBSS/BSA supplemented with 1 mM of EDTA (Sigma, Cat# E9884)

(HBSS/BSA/EDTA), and FBS (Thermofisher, cat# 10437036) were brought to room temperature overnight. PBMCs were isolated on 15 ml of low density Ficoll 1077 in a 50 ml conical tube, and total leukocytes were separated on 15ml of higher density Ficoll 1119 distributed across 7 conical tubes. Blood was first pooled and diluted with HBSS/BSA in a 1:1 ratio, and 25 ml of diluted blood was carefully layered on Ficoll and then centrifuged immediately at 700 x g for 30 minutes (no brake) in a horizontal rotor (swing-out head) tabletop centrifuge, at room temperature. Immediately after centrifugation, cells at the interface were collected and washed in 50 ml HBSS/BSA and centrifuged at 700 x g for 10 minutes. Supernatants were discarded and leukocyte pellets washed again in HBSS/BSA/EDTA and centrifuged at 700 x g for 10 minutes to limit platelet contamination. Low concentration EDTA (1mM) was used to prevent cell-cell adhesion or platelet activation, but a higher concentration was not used to avoid perturbing downstream mitochondrial assays.

To perform cell count, both i) PBMCs (1:10 dilution) and ii) total leukocytes (1:100 dilution) were resuspended in 1 ml of HBSS/BSA/EDTA and counted on the Countess II FL Automated Cell Counter (Thermo Fisher Scientific, Cat# AMQAF1000) in a 1:1 dilution with trypan blue. Counts were performed in duplicates. If the difference between duplicates >10%, the count was repeated and the grand mean of the cell counts taken. Pellets of 5 million PBMCs were aliquoted and frozen at -80°C for mitochondrial assays.

Immunolabeling of cell surface markers

Two antibody cocktails meant for i) cell counting (Cocktail 1) and ii) cell sorting (Cocktail 2), were prepared for fluorescence-activated cell sorting (FACS) (see Supplemental Table 4 for details). Antibodies were gently mixed, kept at 4°C, and shielded from light to avoid bleaching. Cocktail 1 (containing cell surface markers for activated T lymphocytes) was prepared with 17.5 ul HBSS/BSA/EDTA and 2.5 ul per antibody (13 markers, 32.5 ul total antibody mix), for a total of 50 ul. Cocktail 2 was prepared with 200 ul HBSS/BSA/EDTA and 25 ul per antibody (12 markers, 300 ul total sorting antibody mix), for a total of 500 ul.

Prior to each study visit, cell collection tubes (Cat#: 352063, polypropylene, 5 ml) were coated with 4.5ml of DMEM/10% FBS media to minimize cell-tube adhesion and maximize the recovery of sorted cells. Tubes were incubated for 24 hours at room temperature and stored at 4°C until use, and decanted prior to use. Two coated polypropylene tubes were used for the FACS-ready antibody-labeled leukocytes, and an additional 60 coated polypropylene falcon tubes were decanted and 500 ul of media (DMEM/10% FBS) was added to receive sorted cells.

Prior to immunolabeling, total leukocytes were incubated with blocking buffer (to block non-specific binding to FC receptors) at a 1:10 dilution and incubated at room temperature for 10 minutes. A 2 million cell aliquot was diluted to a final volume of 100 ul with HBSS/BSA/EDTA and combined with 50 ul of Cocktail 1. The remainder of total leukocytes (~100M cells) were incubated with 500 ul of Cocktail 2 for 20 minutes in the dark, at room temperature. Both cell preparations were then washed with 5 ml of HBSS/BSA/EDTA and centrifuged at 700 x g for 5 minutes. Using the propylene tubes, Cocktail 1 cells were resuspended in 200 ul of HBSS/BSA/EDTA, and total leukocytes for FACS were resuspended to final concentration of 20 million cells/ml with HBSS/BSA/EDTA.

Fluorescence-activated cell sorting (FACS)

Cells labeled with the Cocktail 1 (counting) panel was only used for data acquisition and phenotype analysis. Cells labeled with the Cocktail 2 (sorting) panel was FACS sorted using a BD™ Influx cell sorter to isolate the subpopulations from peripheral blood. The sorter was controlled using BD FACS Sortware. Cells were sorted using 100 um size nozzle and under the sheath pressure of 20 psi. Sorting speed was kept around 11,000-12,000 events/second. Cell concentration for sorting was measured at about $15x10^6$ cells per ml. Cell sorter drop frequency was 37 KHz, stream focus was 10%, maximum drop charge was 110 Volts. A six-way sorting, 1.0 drop pure sort mode was used to sort the cell subpopulations. Stream deflections were -84, -65, -32, 32, 65, and 84 for six-way sort from left to right. For each participant, 1 million cells (Cocktail 1 panel) were run first to calculate the potential yield of each subpopulation, including neutrophils, B cells monocytes, NK cells, naïve $CD4^+$ and $CD8^+$, CM $CD4^+$ and $CD8^+$, EM $CD4^+$ and $CD8^+$, and TEMRA $CD4^+$ and $CD8^+$ (total cell number x percentage of each subpopulation). The six most abundant subpopulations were sorted. Purity checks were performed on all sorted subpopulations to ensure the instrument performance was good enough to reach the sorted population purity >95%. Raw data (.fcs file) was exported for further analysis on FCS Express 7 research version.

Processing and storage of sorted cells

Following flow cytometry, sorted cell subtypes were transferred and pooled by pipetting about half of each collection tube (2.5 ml) into larger falcon tubes, gently vortexing to liberate cells that may have adhered to the tube wall, and the remaining volume pipetted into the transfer tube. HBSS/2% BSA was used as necessary to equilibrate and cells were centrifuged at 1,000 x g for 5 minutes. Following centrifugation, each cell pellet was isolated by gently decanting the supernatant and re-suspended into 1ml of HBSS/2% BSA. The resulting purified cell suspensions were transferred to a 1.5 ml Eppendorf tube for each cell type, centrifuged at 2,000 x g for 2

minutes at 4°C, and the supernatant carefully removed to leave a dry cell pellet. Samples were stored in liquid nitrogen for 4-12 months (-170°C) until mitochondrial biochemistry and mtDNAcn analyses were performed as a single batch.

Mitochondrial enzymatic activities

Samples were thawed and homogenized in preparation for enzymatic activity measurements with one tungsten bead and 500 ul of homogenization buffer (1 mM EDTA, 50 mM Triethanolamine). Tubes were transferred to a pre-chilled rack and homogenized using a Tissue Lyser (Qiagen cat# 85300) at 30 cycles/second for 1 minute. Samples were then incubated for 5 minutes at 4°C, and homogenization was repeated for 1 minute and the samples were returned to ice ready for enzymatic assays.

Mitochondrial enzyme activities were quantified spectrophotometrically for citrate synthase (CS), cytochrome c oxidase (COX, Complex IV), succinate dehydrogenase (SDH, Complex II), and NADH dehydrogenase (Complex I) as described previously (Picard et al., 2018) with minor modifications. Each sample was measured in triplicates for each enzymatic assay (3 wells for total activity and 3 wells for non-specific activity, except for the COX assay where a single non-specific activity value is determined across 30 wells). Homogenate volumes used for each reaction were: CS: 10 ul, COX and SDH: 20 ul, Complex I: 15 ul.

CS activity was measured by detecting the increase in absorbance at 412 nm, in a reaction buffer (200 mM Tris, pH 7.4) containing acetyl-CoA 0.2 mM, 0.2 mM 5,5'- dithiobis-(2-nitrobenzoic acid) (DTNB), 0.55 mM oxaloacetic acid, and 0.1% Triton X-100. Final CS activity was obtained by integrating OD^{412} change from 150-480 sec, and by subtracting the non-specific activity measured in the absence of oxaloacetate. COX activity was measured by detecting the decrease in absorbance at 550 nm, in a 100 mM potassium phosphate reaction buffer (pH 7.5) containing 0.1% n-dodecylmaltoside and 100 μM of purified reduced cytochrome c. Final COX activity was obtained by integrating OD^{550} change over 200-600 sec and by subtracting spontaneous cyt c oxidation without cell lysate. SDH activity was measured by detecting the decrease in absorbance at 600 nm, in potassium phosphate 100 mM reaction buffer (pH 7.5) containing 2 mM EDTA, 1 mg/ml bovine serum albumin (BSA), 4 μM rotenone, 10 mM succinate, 0.25 mM potassium cyanide, 100 μM decylubuquinone, 100 μM DCIP, 200 μM ATP, 0.4 μM antimycin A. Final SDH activity was obtained by integrating OD^{600} change over 200-900 sec and by subtracting activity detected in the presence of malonate (5 mM), a specific inhibitor of SDH. Complex I activity was measured by detecting the decrease in absorbance at 600 nm, in potassium phosphate 100 mM

reaction buffer (pH 7.5) containing 2 mM EDTA, 3.5 mg/ml bovine serum albumin (BSA), 0.25 mM potassium cyanide, 100 μM decylubuquinone, 100 μM DCIP, 200 μM NADH, 0.4 μM antimycin A. Final Complex I activity was obtained by integrating OD^{600} change over 120-600 sec and by subtracting activity detected in the presence of rotenone (500 μM) and piericidin A (200 μM), specific inhibitors of Complex I. All assays were performed at 30°C. The molar extinction coefficients used were 13.6 L $mol^{-1}cm^{-1}$ for DTNB, 29.5 L $mol^{-1}cm^{-1}$ for reduced cytochrome c, and 16.3 L $mol^{-1}cm^{-1}$ for DCIP to transform change in OD into enzyme activity.

Mitochondrial enzymatic activities were measured on a total of 340 samples, including 136 replicates of the same cell type for the same person. This provided more stable estimates of enzymatic activities than single measures would for a total of 204 individual person-cell combinations. The technical variation for each enzyme varied according to cell type, with cell types with lower enzymatic activities generally showing the highest coefficient of variation (C.V.). C.V. averaged across all cell types were: CS = 6.3%, Complex I = 16.6%, SDH = 9.3%, COX = 23.4% (Supplemental Table 3).

Mitochondrial DNA copy number

mtDNAcn was determined as described previously (Picard et al., 2018) with minor modifications. The same homogenate used for enzymatic measurements (20 ul) was lysed in lysis buffer (100 mM Tris HCl pH 8.5, 0.5% Tween 20, and 200 ug/ml proteinase K) for 10 hours at 55°C followed by inactivation at 95°C for 10 minutes. Five ul of the lysate was directly used as template DNA for measurements of mtDNA copy number. qPCR reactions were set up in triplicates using a liquid handling station (ep-Motion5073, Eppendorf) in 384 well qPCR plates. Duplex qPCR reactions with Taqman chemistry were used to simultaneously quantify mitochondrial and nuclear amplicons in the same reactions. *Master Mix₁* for ND1 (mtDNA) and B2M (nDNA) included: TaqMan Universal Master mix fast (life technologies #4444964), 300 nM of primers and 100 nM probe (ND1-Fwd: GAGCGATGGTGAGAGCTAAGGT, ND1-Rev: CCCTAAAACCCGCCACATCT, Probe:HEX-CCATCACCCTCTACATCACCGCCC-3IABkFQ.B2M-Fwd:CCAGCAGAGAATGGAAAGTCAA,B2M-Rev: TCTCTCTCCATTCTTCAGTAAGTCAACT, Probe:FAM-ATGTGTCTGGGTTTCATCCATCCGACA-3IABkFQ). *Master Mix₂* for COX1 (mtDNA) and RnaseP (nDNA) included: TaqMan Universal Master Mix fast, 300 nM of primers and 100 nM probe (COX1-Fwd: CTAGCAGGTGTCTCCTCTATCT, COX1-Rev: GAGAAGTAGGACTGCTGTGATTAG, Probe: FAM-TGCCATAACCCAATACCAAACGCC-3IABkFQ. RnaseP-Fwd: AGATTTGGACCTGCGAGCG, RnaseP-Rev:

GAGCGGCTGTCTCCACAAGT, Probe: FAM-TTCTGACCTGAAGGCTCTGCGCG-3IABkFQ. The samples were then cycled in a QuantStudio 7 flex qPCR instrument (Applied Biosystems Cat# 4485701) at 50°C for 2 min, 95°C for 20 sec, 95°C for 1 min, 60°C for 20 sec for 40x cycles. Reaction volumes were 20 ul. To ensure comparable Ct values across plates and assays, thresholds for fluorescence detection for both mitochondrial and nuclear amplicons were set to 0.08.

mtDNAcn was calculated using the ΔCt method. The ΔCt was obtained by subtracting the average mtDNA Ct values from the average nDNA Ct values for each pair ND1/B2M and COX1/RNaseP. Relative mitochondrial DNA copies are calculated by raising 2 to the power of the ΔCt and then multiplying by 2 to account for the diploid nature of the nuclear genome (mtDNAcn = 2ΔCt x 2). Both ND1 and COX1 yielded highly correlated mtDNAcn and the average of both amplicon pairs was used as mtDNAcn value for each sample. The overall CV across all cell subtypes was 5.1% for mtDNAcn.

Platelet depletion in PBMCs

For this experiment, participants were 9 community-dwelling older adults (mean age = 79, range: 64-89, 4 women and 5 men). The sample included 7 White and 2 African American participants. Exclusion criteria included diseases or disorders affecting the immune system including autoimmune diseases, cancers, immunosuppressive disorders, or chronic, severe infections; chemotherapy or radiation treatment in the 5 years prior to enrollment; unwillingness to undergo venipuncture; immunomodulatory medications including opioids and steroids; or more than two of the following classes of medications: psychotropics, anti-hypertensives, hormones replacement, or thyroid supplements. Participants were recruited from a volunteer subject pool maintained by the University of Kentucky Sanders-Brown Center on Aging. The study was conducted with the approval of the University of Kentucky Institutional Review Board. Blood (20 mL) was collected by venipuncture into heparinized tubes in the morning hours to control for potential circadian variation. PBMCs were isolated from diluted blood by density gradient centrifugation (20 min at 800 x g, brake off) using Histopaque (Sigma, St. Louis, MO). Buffy coats were washed once, and cells were counted using a hemocytometer. PBMCs (20-30M) were cryopreserved in liquid nitrogen in RPMI-1640 (Lonza) + 10% fetal bovine serum (Hyclone) + 10% DMSO (Fisher), until further processing.

For platelet depletion, PBMCs were first thawed at room temperature and centrifuged at 500 x g for 10 minutes. The supernatant was discarded and the cells were resuspended in 2 ml

of Hank's Balanced Salt Sodium (HBSS) without phenol red, calcium and magnesium (Life Technologies, Cat#14175103). Cells were then counted on the Countess II FL Automated Cell Counter (Thermo Fisher Scientific, Cat# AMQAF1000) in a 1:1 dilution with trypan blue. Cells were then divided into 2 aliquots: 1) 10 million cells for total PBMCs; 2) 11 million cells for platelet depletion. The total PBMCs were centrifuged at 2,000 x g for 2 min at 4°C and subsequently frozen as a dry pellet at -80°C until processing for enzymatic assays and qPCR. The PBMCs destined for platelet deletion cells were processed immediately.

The total PBMCs cell preparation was first immunolabeled with magnetically-coupled antibodies against the platelet marker CD61. The 11 million platelet-depleted PBMCs were then centrifuged at 300 x g for 10 minutes. After spin, the supernatant was aspirated and cells were resuspended in 80 ul of HBSS. Then 20 ul of the CD61 MicroBeads (Miltenyi Biotec, Cat# 130-051-101) were added to the cells and incubated for 15 minutes at 4°C to magnetically label platelets. Cells were washed with 2 ml of HBSS and centrifuged at 300 x g for 10 minutes. The LS column (Miltenyi Biotec, Cat# 130-042-401) was placed in the magnetic field of the MACS Separator (Miltenyi Biotec, Cat# 130-091-051). The LS column was equilibrated with HBSS, cells resuspended in 500 ul of HBSS were applied to the LS column, and the CD61- cells were flown through the column and collected in a 15 ml collection tube. The LS column was then washed 3x with 500 ul of HBSS. The flow through was then spun at 500 x g for 10 minutes, the cell pellet was resuspended in 2 ml of HBSS and re-counted to isolate 10 M platelet-depleted cells. These cells were pelleted at 2,000 x g for 10 minutes at 4°C, the supernatant removed, and cell pellet stored at -80°C. The platelets (CD61^{+}) were recovered by flushing 1 ml of HBSS though the LS column with the plunger in a new tube, centrifuged at 3,000 x g for 10 minutes, the supernatant removed, and the cell pellet stored at -80°C until all samples could be processed for enzymatic activity assays as a single batch. For each participant, this experiment yielded three samples: 1) total PBMCs, 2) platelet depleted PBMCs, and 3) enriched platelets. Each sample was processed in parallel for RC enzymatic activity assays and mtDNAcn as described above.

Statistical analyses

To adjust for potential order effects across the 340 samples (31 samples per 96-well plate, 17 plates total) a linear adjustment was applied to raw values enzymatic activity measures, which adjusts for potential storage and batch effects, ensuring consistency between the first and last samples assayed. Samples from both the cohort and repeat participant were processed and analyzed as a single batch.

Mann-Whitney T tests were used to compare sex differences in cell type proportions and mitochondrial measures. Throughout, effect sizes between groups were computed as Hedges' g (g) to quantify the magnitude of group differences in cell type proportions and mitochondrial measures (by sex, mitotype cell subtype and inter-individual differences). Spearman's r (r) was used to assess strength of associations between continuous variables such as age and cell proportion or age and mitochondrial measures. To assess to what extent mitochondrial features are correlated across cell subtypes (co-regulation) and to calculate the average correlation across mitotypes, Spearman's r matrixes were first computed and transformed to Fisher's Z', and then averaged before transforming back to Spearman's r ($r_{z'}$). One-way non-parametric ANOVA Kruskal-Wallis with post-hoc Dunn's multiple comparison tests were used to compare cell type mitochondrial measures in different cell subtypes and PBMCs. Between- and within-person variation were characterized using coefficients of variation (C.V.). The root mean square of successive differences (rMSSD) was computed to quantify the magnitude of variability between successive weeks for repeated measures. Chi-square tests were computed to compare proportion of mitotype indices categories (enzyme activity per CS, enzyme ratios, enzyme per mtDNA, enzyme per mtDNA density, and enzyme per mtDNA relative to mtDNA density) by age (lower vs higher with increased age) and sex (lower vs higher in men). Finally, one-way non-parametric Friedman tests with post hoc Dunn's multiple comparisons were used to compare mitochondrial measures in platelet-depleted PBMCs, enriched platelets PBMCs, and total PBMCs. Statistical analyses were performed with Prism 8 (GraphPad, CA), R version 4.0.2 and RStudio version 1.3.1056. Statistical significance was set at $p<0.05$.

Data Availability

Further information and requests for resources should be directed to and will be fulfilled by the corresponding author. The raw datasets generated and analyzed in this study are available upon reasonable request.

Acknowledgements

Work of the authors is supported by the Wharton Fund and NIH grants MH119336, GM119793, MH122706, AG066828, AG056635, AG026307, and UL1TR001873. These studies used the resources of the Irving Cancer Center Core Facility funded in part through center grant P30CA013696.

Author contributions

C.T., R.G.R., K.R.K., S.H., and M.P. designed research. S.R., C.T. and A.M. recruited participants. S.R., M.A.M., and W.W. processed samples and collected data. S.R., C.T, A.J., S.C.S, R.G.R. analyzed and interpreted data. S.R. and M.P. drafted the manuscript. All authors edited and commented on the final version of the manuscript.

References

Ackermann, K., Revell, V.L., Lao, O., Rombouts, E.J., Skene, D.J., and Kayser, M. (2012). Diurnal rhythms in blood cell populations and the effect of acute sleep deprivation in healthy young men. Sleep *35*, 933-940.

Artyomov, M.N., and Van den Bossche, J. (2020). Immunometabolism in the Single-Cell Era. Cell Metabolism.

Beis, D., von Känel, R., Heimgartner, N., Zuccarella-Hackl, C., Bürkle, A., Ehlert, U., and Wirtz, P.H. (2018). The Role of Norepinephrine and α-Adrenergic Receptors in Acute Stress-Induced Changes in Granulocytes and Monocytes. Psychosom Med *80*, 649-658.

Biino, G., Santimone, I., Minelli, C., Sorice, R., Frongia, B., Traglia, M., Ulivi, S., Di Castelnuovo, A., Gögele, M., Nutile, T., et al. (2013). Age- and sex-related variations in platelet count in Italy: a proposal of reference ranges based on 40987 subjects' data. PloS one *8*, e54289-e54289.

Brand, K. (1985). Glutamine and glucose metabolism during thymocyte proliferation. Pathways of glutamine and glutamate metabolism. Biochem J *228*, 353-361.

Butler, L.M., Metson-Scott, T., Felix, J., Abhyankar, A., Rainger, G.E., Farndale, R.W., Watson, S.P., and Nash, G.B. (2007). Sequential adhesion of platelets and leukocytes from flowing whole blood onto a collagen-coated surface: requirement for a GpVI-binding site in collagen. Thromb Haemost *97*, 814-821.

Calvo, S.E., Clauser, K.R., and Mootha, V.K. (2016). MitoCarta2.0: an updated inventory of mammalian mitochondrial proteins. Nucleic Acids Res *44*, D1251-1257.

Cavalcanti-de-Albuquerque, J.P.A., Salvador, I.C., Martins, E.L., Jardim-Messeder, D., Werneck-de-Castro, J.P.S., Galina, A., and Carvalho, D.P. (2014). Role of estrogen on skeletal muscle mitochondrial function in ovariectomized rats: a time course study in different fiber types. Journal of Applied Physiology *116*, 779-789.

Chacko, B.K., Kramer, P.A., Ravi, S., Johnson, M.S., Hardy, R.W., Ballinger, S.W., and Darley-Usmar, V.M. (2013). Methods for defining distinct bioenergetic profiles in platelets, lymphocytes, monocytes, and neutrophils, and the oxidative burst from human blood. Lab Invest *93*, 690-700.

Chacko, B.K., Zhi, D., Darley-Usmar, V.M., and Mitchell, T. (2016). The Bioenergetic Health Index is a sensitive measure of oxidative stress in human monocytes. Redox Biol *8*, 43-50.

Dhabhar, F.S., Malarkey, W.B., Neri, E., and McEwen, B.S. (2012). Stress-induced redistribution of immune cells--from barracks to boulevards to battlefields: a tale of three hormones--Curt Richter Award winner. Psychoneuroendocrinology *37*, 1345-1368.

Dhabhar, F.S., Miller, A.H., Stein, M., McEwen, B.S., and Spencer, R.L. (1994). Diurnal and Acute Stress-Induced Changes in Distribution of Peripheral Blood Leukocyte Subpopulations. Brain, Behavior, and Immunity *8*, 66-79.

Dixon, N., Li, T., Marion, B., Faust, D., Dozier, S., Molina, A., Rudnick, S., and Bonkovsky, H.L. (2019). Pilot study of mitochondrial bioenergetics in subjects with acute porphyrias. Mol Genet Metab *128*, 228-235.

Furman, D., Hejblum, B.P., Simon, N., Jojic, V., Dekker, C.L., Thiébaut, R., Tibshirani, R.J., and Davis, M.M. (2014). Systems analysis of sex differences reveals an immunosuppressive role for testosterone in the response to influenza vaccination. Proc Natl Acad Sci U S A *111*, 869-874.

Gan, Z., Fu, T., Kelly, D.P., and Vega, R.B. (2018). Skeletal muscle mitochondrial remodeling in exercise and diseases. Cell Research *28*, 969-980.

Giordano, C., Iommarini, L., Giordano, L., Maresca, A., Pisano, A., Valentino, M.L., Caporali, L., Liguori, R., Deceglie, S., Roberti, M., et al. (2014). Efficient mitochondrial biogenesis drives incomplete penetrance in Leber's hereditary optic neuropathy. Brain *137*, 335-353.

Hebert, S.L., Marquet-de Rougé, P., Lanza, I.R., McCrady-Spitzer, S.K., Levine, J.A., Middha, S., Carter, R.E., Klaus, K.A., Therneau, T.M., Highsmith, E.W., et al. (2015). Mitochondrial Aging and Physical Decline: Insights From Three Generations of Women. J Gerontol A Biol Sci Med Sci *70*, 1409-1417.

Hurtado-Roca, Y., Ledesma, M., Gonzalez-Lazaro, M., Moreno-Loshuertos, R., Fernandez-Silva, P., Enriquez, J.A., and Laclaustra, M. (2016). Adjusting MtDNA Quantification in Whole Blood for Peripheral Blood Platelet and Leukocyte Counts. PLOS ONE *11*, e0163770.

Iershov, A., Nemazanyy, I., Alkhoury, C., Girard, M., Barth, E., Cagnard, N., Montagner, A., Chretien, D., Rugarli, E.I., Guillou, H., et al. (2019). The class 3 PI3K coordinates autophagy and mitochondrial lipid catabolism by controlling nuclear receptor PPARα. Nature Communications *10*, 1566.

Jang, J.Y., Blum, A., Liu, J., and Finkel, T. (2018). The role of mitochondria in aging. The Journal of Clinical Investigation *128*, 3662-3670.

Jones, N., Vincent, E.E., Cronin, J.G., Panetti, S., Chambers, M., Holm, S.R., Owens, S.E., Francis, N.J., Finlay, D.K., and Thornton, C.A. (2019). Akt and STAT5 mediate naïve human CD4+ T-cell early metabolic response to TCR stimulation. Nature Communications *10*, 2042.

Karabatsiakis, A., Böck, C., Salinas-Manrique, J., Kolassa, S., Calzia, E., Dietrich, D.E., and Kolassa, I.T. (2014). Mitochondrial respiration in peripheral blood mononuclear cells correlates with depressive subsymptoms and severity of major depression. Translational Psychiatry *4*, e397-e397.

Karan, K.R., Trumpff, C., McGill, M.A., Thomas, J.E., Sturm, G., Lauriola, V., Sloan, R.P., Rohleder, N., Kaufman, B.A., Marsland, A.L., et al. (2020). Mitochondrial respiratory capacity modulates LPS-induced inflammatory signatures in human blood. Brain, Behavior, & Immunity - Health *5*, 100080.

Khalifa, A.R.M., Abdel-Rahman, E.A., Mahmoud, A.M., Ali, M.H., Noureldin, M., Saber, S.H., Mohsen, M., and Ali, S.S. (2017). Sex-specific differences in mitochondria biogenesis, morphology, respiratory function, and ROS homeostasis in young mouse heart and brain. Physiol Rep *5*, e13125.

Larsen, S., Nielsen, J., Hansen, C.N., Nielsen, L.B., Wibrand, F., Stride, N., Schroder, H.D., Boushel, R., Helge, J.W., Dela, F., et al. (2012). Biomarkers of mitochondrial content in skeletal muscle of healthy young human subjects. J Physiol *590*, 3349-3360.

Lindquist, C., Bjørndal, B., Rossmann, C.R., Svardal, A., Hallström, S., and Berge, R.K. (2018). A fatty acid analogue targeting mitochondria exerts a plasma triacylglycerol lowering effect in rats with impaired carnitine biosynthesis. PLoS One *13*, e0194978.

Makowski, L., Chaib, M., and Rathmell, J.C. (2020). Immunometabolism: From basic mechanisms to translation. Immunol Rev *295*, 5-14.

Meier, H.C.S., Sandler, D.P., Simonsick, E.M., Weng, N.P., and Parks, C.G. (2020). Sex differences in the association between antinuclear antibody positivity with diabetes and multimorbidity in older adults: Results from the Baltimore Longitudinal Study of Aging. Exp Gerontol, 110906.

Mengel-From, J., Thinggaard, M., Dalgård, C., Kyvik, K.O., Christensen, K., and Christiansen, L. (2014). Mitochondrial DNA copy number in peripheral blood cells declines with age and is associated with general health among elderly. Hum Genet *133*, 1149-1159.

Michalek, R.D., Gerriets, V.A., Jacobs, S.R., Macintyre, A.N., MacIver, N.J., Mason, E.F., Sullivan, S.A., Nichols, A.G., and Rathmell, J.C. (2011). Cutting edge: distinct glycolytic and lipid oxidative metabolic programs are essential for effector and regulatory CD4+ T cell subsets. J Immunol *186*, 3299-3303.

Moore, A.Z., Ding, J., Tuke, M.A., Wood, A.R., Bandinelli, S., Frayling, T.M., and Ferrucci, L. (2018). Influence of cell distribution and diabetes status on the association between mitochondrial DNA copy number and aging phenotypes in the InCHIANTI study. Aging Cell *17*, e12683.

Nicoli, F., Papagno, L., Frere, J.J., Cabral-Piccin, M.P., Clave, E., Gostick, E., Toubert, A., Price, D.A., Caputo, A., and Appay, V. (2018). Naïve CD8+ T-Cells Engage a Versatile Metabolic Program Upon Activation in Humans and Differ Energetically From Memory CD8+ T-Cells. Frontiers in Immunology *9*.

Nikolich-Žugich, J. (2014). Aging of the T cell compartment in mice and humans: from no naive expectations to foggy memories. J Immunol *193*, 2622-2629.

Nomura, M., Liu, J., Rovira, I.I., Gonzalez-Hurtado, E., Lee, J., Wolfgang, M.J., and Finkel, T. (2016). Fatty acid oxidation in macrophage polarization. Nature immunology *17*, 216-217.

Pagliarini, D.J., Calvo, S.E., Chang, B., Sheth, S.A., Vafai, S.B., Ong, S.E., Walford, G.A., Sugiana, C., Boneh, A., Chen, W.K., et al. (2008). A mitochondrial protein compendium elucidates complex I disease biology. Cell *134*, 112-123.

Patin, E., Hasan, M., Bergstedt, J., Rouilly, V., Libri, V., Urrutia, A., Alanio, C., Scepanovic, P., Hammer, C., Jönsson, F., et al. (2018). Natural variation in the parameters of innate immune cells is preferentially driven by genetic factors. Nature Immunology *19*, 302-314.

Pearce, E.L., Poffenberger, M.C., Chang, C.-H., and Jones, R.G. (2013). Fueling Immunity: Insights into Metabolism and Lymphocyte Function. Science *342*, 1242454.

Picard, M., Hepple, R.T., and Burelle, Y. (2012a). Mitochondrial functional specialization in glycolytic and oxidative muscle fibers: tailoring the organelle for optimal function. Am J Physiol Cell Physiol *302*, C629-641.

Picard, M., Jung, B., Liang, F., Azuelos, I., Hussain, S., Goldberg, P., Godin, R., Danialou, G., Chaturvedi, R., Rygiel, K., et al. (2012b). Mitochondrial dysfunction and lipid accumulation in the human diaphragm during mechanical ventilation. Am J Respir Crit Care Med *186*, 1140-1149.

Picard, M., and McEwen, B.S. (2018). Psychological Stress and Mitochondria: A Systematic Review. Psychosom Med *80*, 141-153.

Picard, M., Prather, A.A., Puterman, E., Cuillerier, A., Coccia, M., Aschbacher, K., Burelle, Y., and Epel, E.S. (2018). A Mitochondrial Health Index Sensitive to Mood and Caregiving Stress. Biol Psychiatry *84*, 9-17.

Picard, M., Trumpff, C., and Burelle, Y. (2019). Mitochondrial psychobiology: foundations and applications. Curr Opin Behav Sci *28*, 142-151.

Picard, M., Wallace, D.C., and Burelle, Y. (2016). The rise of mitochondria in medicine. Mitochondrion *30*, 105-116.

Ron-Harel, N., Ghergurovich, J.M., Notarangelo, G., LaFleur, M.W., Tsubosaka, Y., Sharpe, A.H., Rabinowitz, J.D., and Haigis, M.C. (2019). T Cell Activation Depends on Extracellular Alanine. Cell Rep *28*, 3011-3021.e3014.

Segerstrom, S.C., Sephton, S.E., and Westgate, P.M. (2017). Intraindividual variability in cortisol: Approaches, illustrations, and recommendations. Psychoneuroendocrinology *78*, 114-124.

Short, K.R., Bigelow, M.L., Kahl, J., Singh, R., Coenen-Schimke, J., Raghavakaimal, S., and Nair, K.S. (2005). Decline in skeletal muscle mitochondrial function with aging in humans. Proc Natl Acad Sci U S A *102*, 5618-5623.

Silaidos, C., Pilatus, U., Grewal, R., Matura, S., Lienerth, B., Pantel, J., and Eckert, G.P. (2018). Sex-associated differences in mitochondrial function in human peripheral blood mononuclear cells (PBMCs) and brain. Biology of Sex Differences *9*, 34.

Torres, M.J., Ryan, T.E., Lin, C.T., Zeczycki, T.N., and Neufer, P.D. (2018). Impact of 17β-estradiol on complex I kinetics and H(2)O(2) production in liver and skeletal muscle mitochondria. J Biol Chem *293*, 16889-16898.

Turner, N., Bruce, C.R., Beale, S.M., Hoehn, K.L., So, T., Rolph, M.S., and Cooney, G.J. (2007). Excess lipid availability increases mitochondrial fatty acid oxidative capacity in muscle: evidence against a role for reduced fatty acid oxidation in lipid-induced insulin resistance in rodents. Diabetes *56*, 2085-2092.

van der Windt, G.J., Everts, B., Chang, C.H., Curtis, J.D., Freitas, T.C., Amiel, E., Pearce, E.J., and Pearce, E.L. (2012). Mitochondrial respiratory capacity is a critical regulator of CD8+ T cell memory development. Immunity *36*, 68-78.

van der Windt, G.J.W., O'Sullivan, D., Everts, B., Huang, S.C.-C., Buck, M.D., Curtis, J.D., Chang, C.-H., Smith, A.M., Ai, T., Faubert, B., et al. (2013). CD8 memory T cells have a bioenergetic advantage that underlies their rapid recall ability. Proceedings of the National Academy of Sciences *110*, 14336.

Ventura-Clapier, R., Piquereau, J., Veksler, V., and Garnier, A. (2019). Estrogens, Estrogen Receptors Effects on Cardiac and Skeletal Muscle Mitochondria. Frontiers in Endocrinology *10*.

Verhoeven, J.E., Révész, D., Picard, M., Epel, E.E., Wolkowitz, O.M., Matthews, K.A., Penninx, B., and Puterman, E. (2018). Depression, telomeres and mitochondrial DNA: between- and within-person associations from a 10-year longitudinal study. Mol Psychiatry *23*, 850-857.

Wallace, Douglas C. (2015). Mitochondrial DNA Variation in Human Radiation and Disease. Cell *163*, 33-38.

Weiss, S.L., Selak, M.A., Tuluc, F., Perales Villarroel, J., Nadkarni, V.M., Deutschman, C.S., and Becker, L.B. (2015). Mitochondrial dysfunction in peripheral blood mononuclear cells in pediatric septic shock. Pediatr Crit Care Med *16*, e4-e12.

Ye, K., Lu, J., Ma, F., Keinan, A., and Gu, Z. (2014). Extensive pathogenicity of mitochondrial heteroplasmy in healthy human individuals. Proceedings of the National Academy of Sciences *111*, 10654.

Yu-Wai-Man, P., Sitarz, K.S., Samuels, D.C., Griffiths, P.G., Reeve, A.K., Bindoff, L.A., Horvath, R., and Chinnery, P.F. (2010). OPA1 mutations cause cytochrome c oxidase deficiency due to loss of wild-type mtDNA molecules. Hum Mol Genet *19*, 3043-3052.

Zhang, J., Li, M., and He, Y. (2015). Large population study for age- and gender- related variations of platelet indices in Southwest China healthy adults. Hematology & Transfusion International Journal *1*.

Zhang, R., Wang, Y., Ye, K., Picard, M., and Gu, Z. (2017). Independent impacts of aging on mitochondrial DNA quantity and quality in humans. BMC Genomics *18*, 890.

Figure Legends

Figure 1 – Immune cell subtype distribution in adult women and men.

(**a**) Overview of participant demographics, blood collection, processing, and analysis pipeline. Total leukocytes were isolated using Ficoll 1119 and PBMCs were isolated on Ficoll 1077. The five mitochondrial features analyzed on the mitochondrial phenotyping platform are colored. (**b**) Stacked histogram showing the leukocytes distribution derived from the complete blood count (CBC). (**c**) Diagram illustrating the proportion of circulating immune cell subtypes (% of all detected cells) quantified by flow cytometry from total peripheral blood leukocytes. Cell surface markers and subtype definitions are detailed in Supplemental Table 1. (**d**) Forest plot of the effect sizes for cell subtype distribution differences between women (n=11) and men (n=10). P-values from non-parametric Mann-Whitney T test. The fold change comparing raw counts between women and men and shown on the right. Error bars reflect the 95% confidence interval (C.I.) on the effect size. (e) Distribution of cell types proportions in women and men illustrating the range of $CD4^+$ and $CD8^+$ naïve cells, B cells, and monocytes, highlighting the natural variation among our cohort. Each datapoint reflects a different individual. (**f**) Spearman's r correlation between age and cell types proportion. n=21, $p<0.05$*, $p<0.01$**.

Figure 2 – Cell subtype differences in mitochondrial content and RC function.

(**a-e**) Violin plots illustrating immune cell type differences in mitochondrial features across cell subtypes and total PBMCs. For each individual, only the 6 most abundant cell types were analyzed (n=21 individuals, 12-18 per cell subtype). Dashed lines are median (thick) and 25th and 75th quartiles (thin). P-values from One-Way non-parametric ANOVA Kruskal-Wallis test, post-hoc Dunn's multiple comparisons relative to PBMCs. (**f**) Spearman's r inter-correlations of mitochondrial features across subtypes. Insets show the scatterplots for selected correlations. $p<0.05$*, $p<0.01$**, $p<0.001$***, $p<0.0001$****.

Figure 3 – Mitochondrial health index (MHI) and coherence of mitochondrial features across cell subtypes.

(**a**) Schematic of the MHI equation reflecting respiratory chain function as the numerator, and markers of mitochondrial content as the denominator, producing a metric of energy production capacity on a per-mitochondrion basis. (**b**) MHI across immune cell subtypes. Dashed lines are median (thick) and 25th and 75th quartiles (thin). P-values from One-Way non-parametric ANOVA Kruskal-Wallis test with Dunn's multiple comparison test of subtypes relative to PBMCs, n=12-18 per cell subtype. (**c**) Correlation matrices showing the association between cell subtypes in

mitochondrial features. Correlations were not computed for cell subtype pairs with fewer than n=6 observations (gray cell). (**d**) Average effect sizes reflecting the within-person coherence of mitochondrial features across cell types (calculated using Fisher z-transformation). $p<0.05$*, $p<0.001$***.

Figure 4 – Associations of mitochondrial features with sex and age across cell subtypes.
(**a-f**) Effect size of sex differences in mitochondrial activity across cell subtypes quantified by Hedges' g. The fold change computed from raw values is shown on the right. P-values from Mann-Whitney test. Error bars reflect the 95% C.I. on the effect size. (**g-l**) Association of age and mitochondrial features across cell subtypes. P-values from Spearman's r correlations, not adjusted for multiple comparisons. n=21 (11 women, 10 men), $p<0.05$*, $p<0.01$**, $p<0.001$***.

Figure 5 – Within-person variability of mitochondrial features across cell subtypes.
(**a**) Overview of the repeat participant design, including blood collection, processing, and analysis. All samples were collected, stored, and processed as a single batch with samples from the cohort. (**b-g**) Natural weekly variation for each mitochondrial feature across cell subtypes in the same person across 9 weeks represented as scaled centered data where 1 unit change represents a one-standard deviation (S.D.) difference. Root mean square of the successive differences (rMSSDs) quantify the magnitude of variability between successive weeks. The coefficients of variation (C.V.) quantify the magnitude of variability across the total 9 weeks. Monocytes and $CD4^+$ CM-EM were not collected on weeks 1 and 2. (**h**) Side-by-side comparison of CS activity between the cohort (n=12-18 per cell subtype) and the repeat participant (n=7-9 time points) across cell subtypes. The dynamic range of two cell subtypes are represented: monocytes and $CD4^+$ naïve T cells. (**i**) Within-person correlation matrices between cell subtypes for each mitochondrial feature over 9 weeks, illustrating to what extent cell subtypes are correlated with each other (co-regulation). (**j**) Average inter-correlation across all cell subtypes by mitochondrial feature (calculated using Fisher z-transformation) indicating the degree of coherence within person. (**k**) Comparison of co-regulation patterns among mitochondrial features between the cohort and the repeat participant. Each datapoint represents a cell subtype pair.

Figure 6 – Mitotypes in purified leukocyte populations from the cohort and repeated-measures.
(**a**) Schematic illustrating the multivariate approach to generate and visualize mitotypes by putting into relation two or more mitochondrial features. Notice the similarity and added insight relative to single metrics, similar to the integration of height and weight into body mass index (BMI). (**b-e**)

Mitotypes plotted for each cell subtype among the cohort. Data are means and SEM. Overlaid shaded areas denote general leukocyte categories. (**f**) Summary of mitotype differences between (*i*) innate and adaptive subdivisions and (*ii*) naïve and memory T cells. (**g-i**) Validation of subtype-specific mitotype differences in the repeat participant, illustrating the conserved nature of mitotypes across individuals. Only the six cell subtypes analyzed in the repeat participant are plotted. (**j**) Comparison of the magnitude of the difference (Hedges' g) in mitotypes between cell types, and between individuals. Dark blue bars indicate the magnitude of the dominant difference in mitotypes between cell subtypes. Light blue bars indicate the magnitude of the difference in mitotypes between the cohort and the repeat participant within a cell type. Error bars reflect the 95% C.I. on the effect size.

Figure 7 – Mitotype distribution and strength of difference across sex and age.

(**a**) Ranking of mitotype indices by their difference between women and men, quantified as the effect size (Hedges' g) between women and men. A total of 16 mitotype indices were generated, subdivided into 5 main color-coded categories (see Supplemental Figure 7). Pie charts illustrate the proportion mitotypes belonging to each category that are either higher in women (left) or in men (right). P-values for enrichment of sexually dimorphic mitotypes are derived from Chi-square test. (**b**) Violin plots illustrating the two mitotypes with the largest opposite sex differences, both showing large effect sizes (g). (**c**) Heatmap of sex differences (Hedges' g) for primary measures of mitochondrial function (top) and multivariate mitotypes (bottom) across cell subtypes. The histogram at the bottom shows the average absolute effect size across all mitotypes (calculated from absolute values). (**d**) Ranking of mitotype indices by the strength and direction of their association with age, with enrichment analysis analyzed as for sex (Chi-square test). (**e**) Spearman's r correlations of mitotypes/cell type combinations with the strongest positive and negative associations with age. (**f**) Heatmap of the age correlations (Spearman's r) for primary features and composite mitotypes across cell subtypes. The histogram at the bottom shows the average effect size (r) for each cell subtype (calculated using absolute values and Fisher z-transformation). $p<0.05$*, $p<0.01$**, $p<0.001$***, $p<0.0001$****.

Figure 8 – Association of blood biomarkers with mitochondrial parameters across cell subtypes and primary mitochondrial features.

(**a**) Overview of blood biochemistry, hormonal, and metabolic biomarkers collected for each participant. (**b**) Sex- and age-adjusted correlations between blood biomarkers and mitochondrial features across cell subtypes for the cohort (n=10-20 per mito-biomarker combinations) shown as a heatmap. (**c**) Same as (b) but using repeated-measures of mitochondrial features and

biomarkers in the repeat participant. (**d**) Scatterplots of the indicated correlations between Neutrophils CS activity and LDL cholesterol (left), and $CD4^+$ CM-EM mtDNAcn and potassium (K^+) (right) for the cohort (top row) and the repeat participant (bottom row). (**e**) Frequency distributions of the aggregated effect sizes between biomarkers and mitochondrial features across cell subtypes for the cohort (total correlation pairs=1,080) and the repeat participant (total correlation pairs=882).

Figure 9 – Influence of cell subtypes on mitochondrial features in total PBMCs.
(**a-b**) Pairwise correlations of cell subtype proportions obtained from cell sorting with mitochondrial features measured in PBMCs for the cohort (n=20) and the repeat participant (n=1 x 9 timepoints). Aggregate correlations are shown as a heatmap (top) and individual scatterplots (bottom). (**c**) Frequency distributions of the effect sizes between PBMC mitochondrial features and cell subtypes proportions for the cohort and the repeat participant (total correlation pairs=72, for both).

Figure 10 – Influence of platelet contamination on mitochondrial features in total PBMCs.
(**a**) Schematic of the natural state of Ficoll-isolated PBMCs associated with contaminating platelets. (**b**) Association of age and circulating platelet abundance (i.e., count) in our cohort (Spearman's r). (**c**) Change in platelet abundance as a function of age. The magnitude of the association (slope of the regression: 10^9 platelets/L per year) from two large epidemiological studies and our cohort. The inset shows the actual regressions (n=21 to 22,351). (**d**) Effect sizes of the association between platelet count and PBMCs mitochondrial features in our cohort (n=20). (**e**) Overview of the experimental PBMC platelet depletion study, yielding three different samples subjected to mitochondrial phenotyping. (**f**) Fold change in mitochondrial parameters between i) platelet-depleted PBMCs and ii) enriched platelets (with contaminating PBMCs) relative iii) total PBMCs. P-values from One-Way non-parametric ANOVA Friedman test, post-hoc Dunn's multiple comparisons relative to total PBMCs. (**g**) Percent change of platelet-depleted PBMCs mitochondrial features from total PBMCs. n=9, $p<0.05$*, $p<0.01$**, $p<0.001$***, $p<0.0001$****.

Figure 1

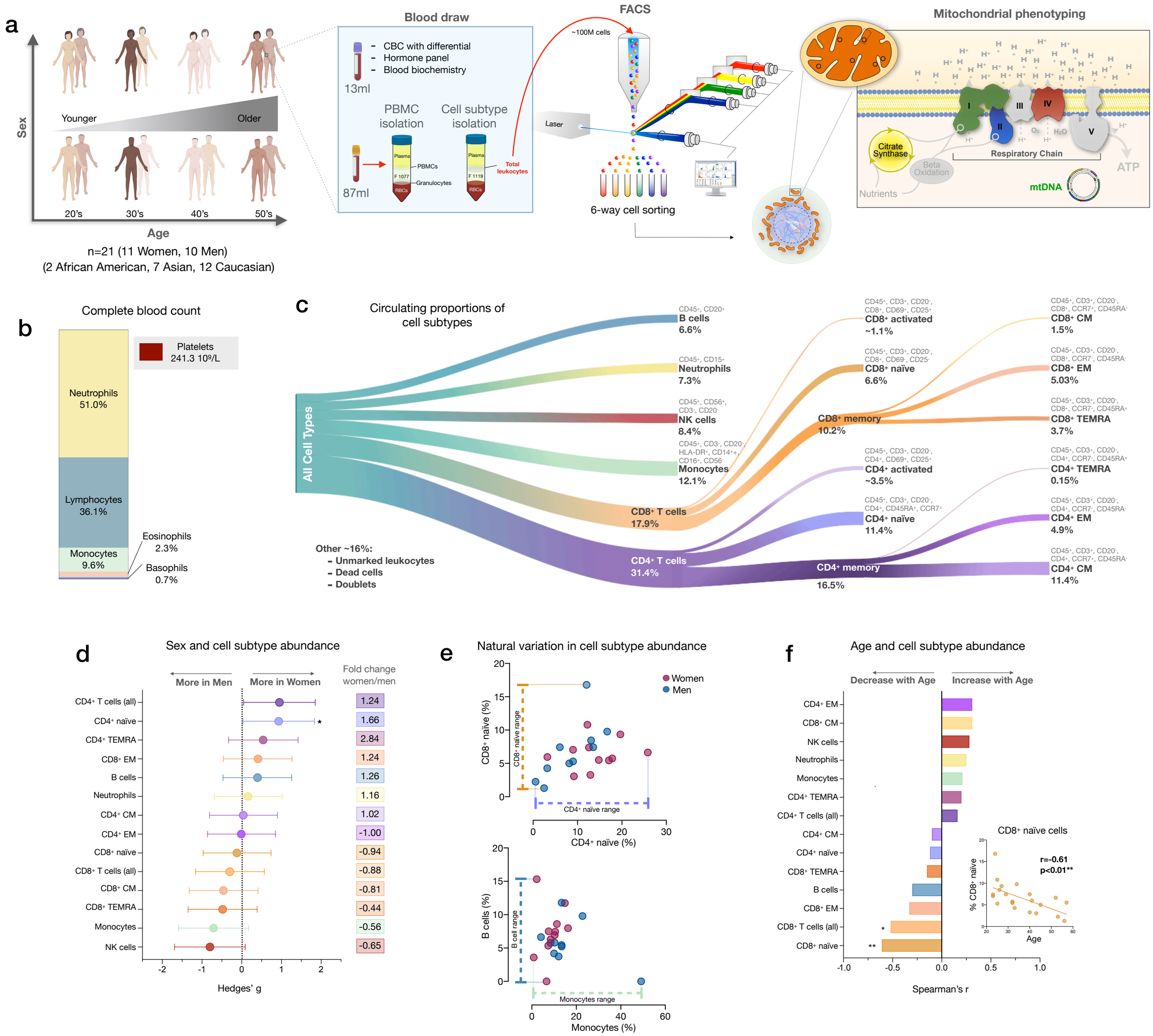

Figure 1 – Immune cell subtype distribution in adult women and men.

(**a**) Overview of participant demographics, blood collection, processing, and analysis pipeline. Total leukocytes were isolated using Ficoll 1119 and PBMCs were isolated on Ficoll 1077. The five mitochondrial features analyzed on the mitochondrial phenotyping platform are colored. (**b**) Stacked histogram showing the leukocytes distribution derived from the complete blood count (CBC). (**c**) Diagram illustrating the proportion of circulating immune cell subtypes (% of all detected cells) quantified by flow cytometry from total peripheral blood leukocytes. Cell surface markers and subtype definitions are detailed in Supplemental Table 1. (**d**) Forest plot of the effect sizes for cell subtype distribution differences between women (n=11) and men (n=10). P-values from non-parametric Mann-Whitney T test. The fold change comparing raw counts between women and men and shown on the right. Error bars reflect the 95% confidence interval (C.I.) on the effect size. (e) Distribution of cell types proportions in women and men illustrating the range of CD4+ and CD8+ naïve cells, B cells, and monocytes, highlighting the natural variation among our cohort. Each datapoint reflects a different individual. (**f**) Spearman's r correlation between age and cell types proportion. n=21, $p<0.05$*, $p<0.01$**.

Figure 2

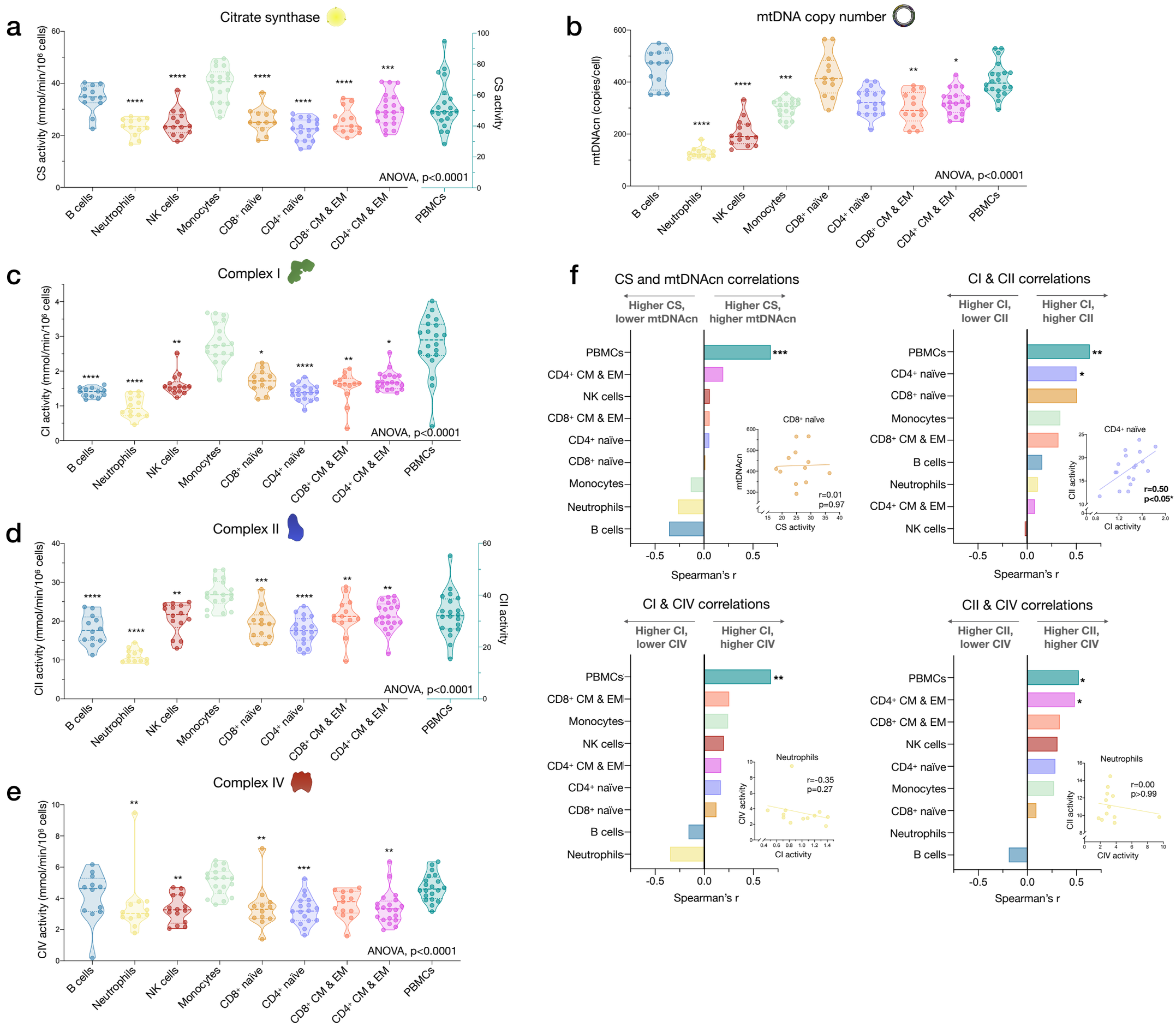

Figure 2 – Cell subtype differences in mitochondrial content and RC function.
(**a-e**) Violin plots illustrating immune cell type differences in mitochondrial features across cell subtypes and total PBMCs. For each individual, only the 6 most abundant cell types were analyzed (n=21 individuals, 12-18 per cell subtype). Dashed lines are median (thick) and 25th and 75th quartiles (thin). P-values from One-Way non-parametric ANOVA Kruskal-Wallis test, post-hoc Dunn's multiple comparisons relative to PBMCs. (**f**) Spearman's r inter-correlations of mitochondrial features across subtypes. Insets show the scatterplots for selected correlations. p<0.05*, p<0.01**, p<0.001***, p<0.0001****.

Figure 3

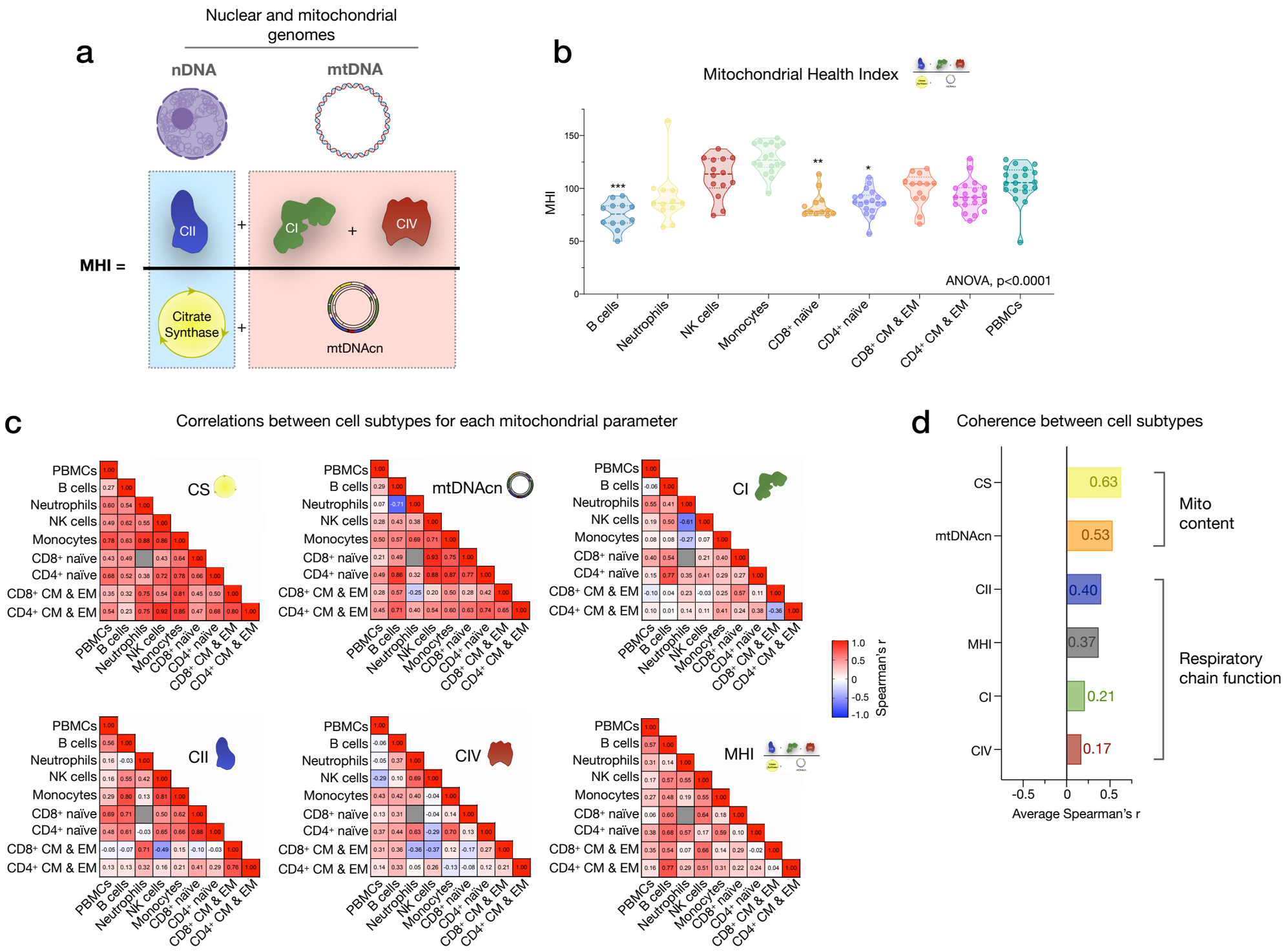

Figure 3 – Mitochondrial health index (MHI) and coherence of mitochondrial features across cell subtypes.
(**a**) Schematic of the MHI equation reflecting respiratory chain function as the numerator, and markers of mitochondrial content as the denominator, producing a metric of energy production capacity on a per-mitochondrion basis. (**b**) MHI across immune cell subtypes. Dashed lines are median (thick) and 25th and 75th quartiles (thin). P-values from One-Way non-parametric ANOVA Kruskal-Wallis test with Dunn's multiple comparison test of subtypes relative to PBMCs, n=12-18 per cell subtype. (**c**) Correlation matrices showing the association between cell subtypes in mitochondrial features. Correlations were not computed for cell subtype pairs with fewer than n=6 observations (gray cell). (**d**) Average effect sizes reflecting the within-person coherence of mitochondrial features across cell types (calculated using Fisher z-transformation). $p<0.05$*, $p<0.001$***.

Figure 4

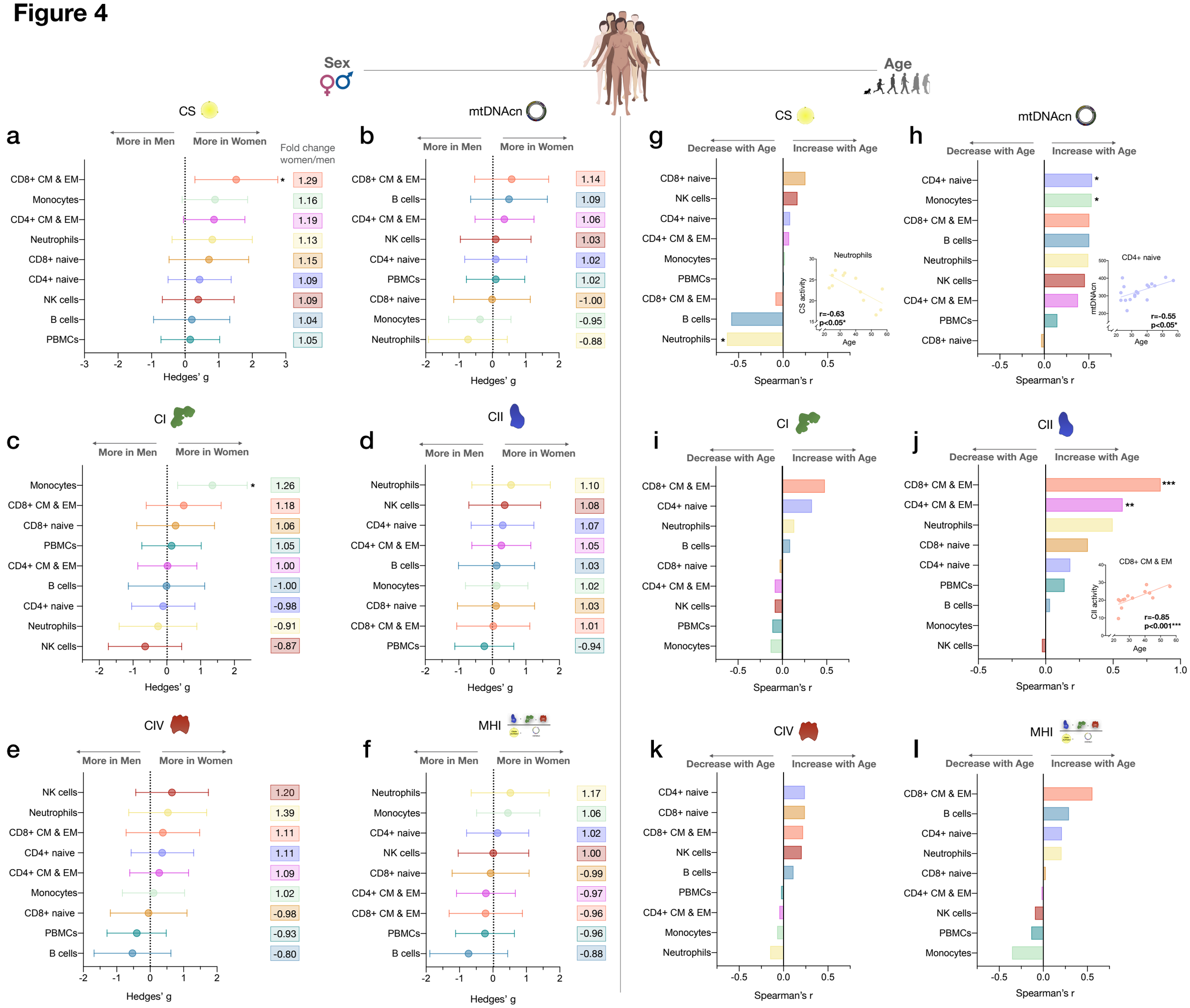

Figure 4 – Associations of mitochondrial features with sex and age across cell subtypes.

(**a-f**) Effect size of sex differences in mitochondrial activity across cell subtypes quantified by Hedges' g. The fold change computed from raw values is shown on the right. P-values from Mann-Whitney test. Error bars reflect the 95% C.I. on the effect size. (**g-l**) Association of age and mitochondrial features across cell subtypes. P-values from Spearman's r correlations, not adjusted for multiple comparisons. n=21 (11 women, 10 men), p<0.05*, p<0.01**, p<0.001***.

Figure 5

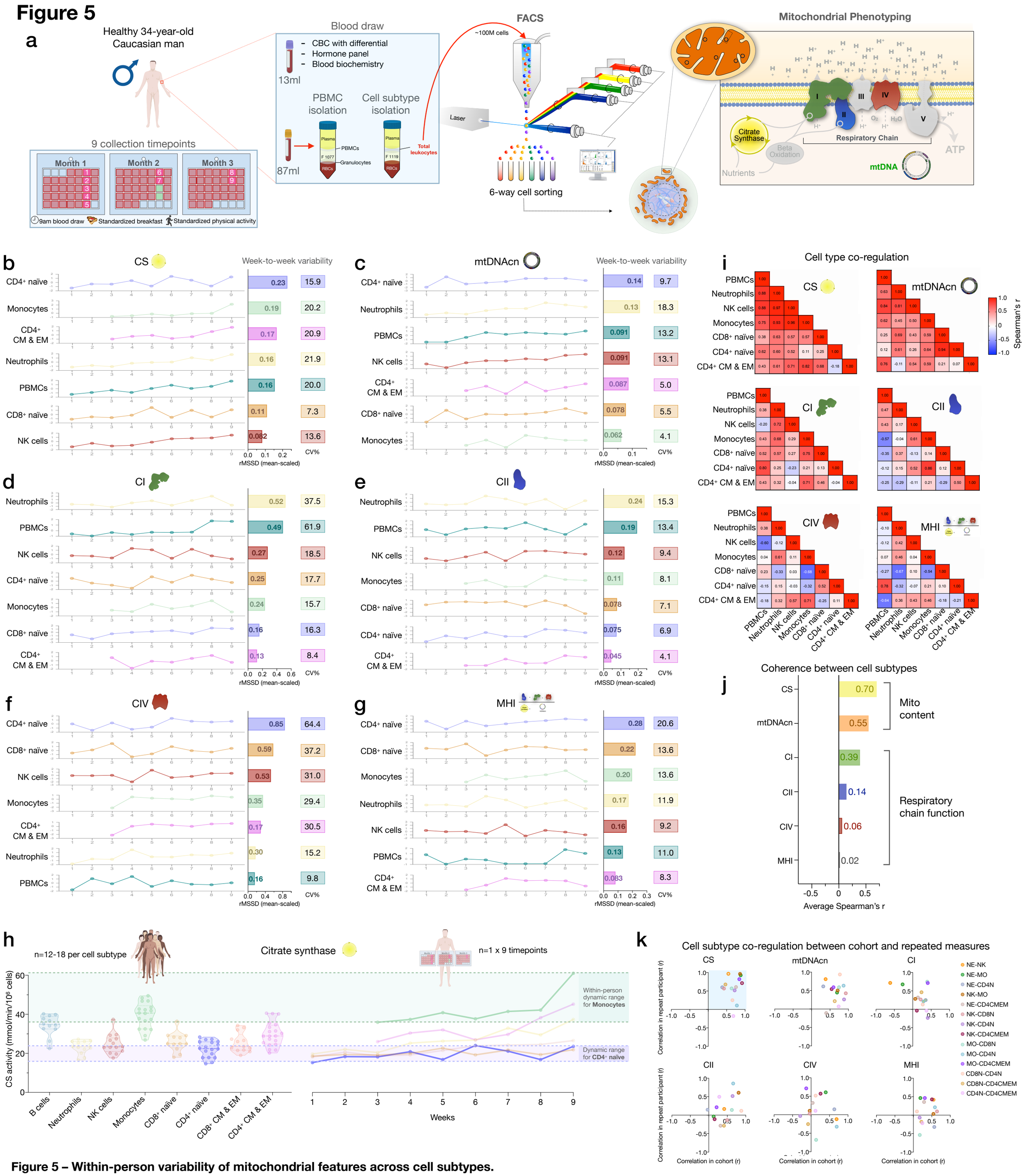

Figure 5 – Within-person variability of mitochondrial features across cell subtypes.

(**a**) Overview of the repeat participant design, including blood collection, processing, and analysis. All samples were collected, stored, and processed as a single batch with samples from the cohort. (**b-g**) Natural weekly variation for each mitochondrial feature across cell subtypes in the same person across 9 weeks represented as scaled centered data where 1 unit change represents a one-standard deviation (S.D.) difference. Root mean square of the successive differences (rMSSDs) quantify the magnitude of variability between successive weeks. The coefficients of variation (C.V.) quantify the magnitude of variability across the total 9 weeks. Monocytes and CD4+ CM-EM were not collected on weeks 1 and 2. (**h**) Side-by-side comparison of CS activity between the cohort (n=12-18 per cell subtype) and the repeat participant (n=7-9 time points) across cell subtypes. The dynamic range of two cell subtypes are represented: monocytes and CD4+ naïve T cells. (**i**) Within-person correlation matrices between cell subtypes for each mitochondrial feature over 9 weeks, illustrating to what extent cell subtypes are correlated with each other (co-regulation). (**j**) Average inter-correlation across all cell subtypes by mitochondrial feature (calculated using Fisher z-transformation) indicating the degree of coherence within person. (**k**) Comparison of co-regulation patterns among mitochondrial features between the cohort and the repeat participant. Each datapoint represents a cell subtype pair.

Figure 6

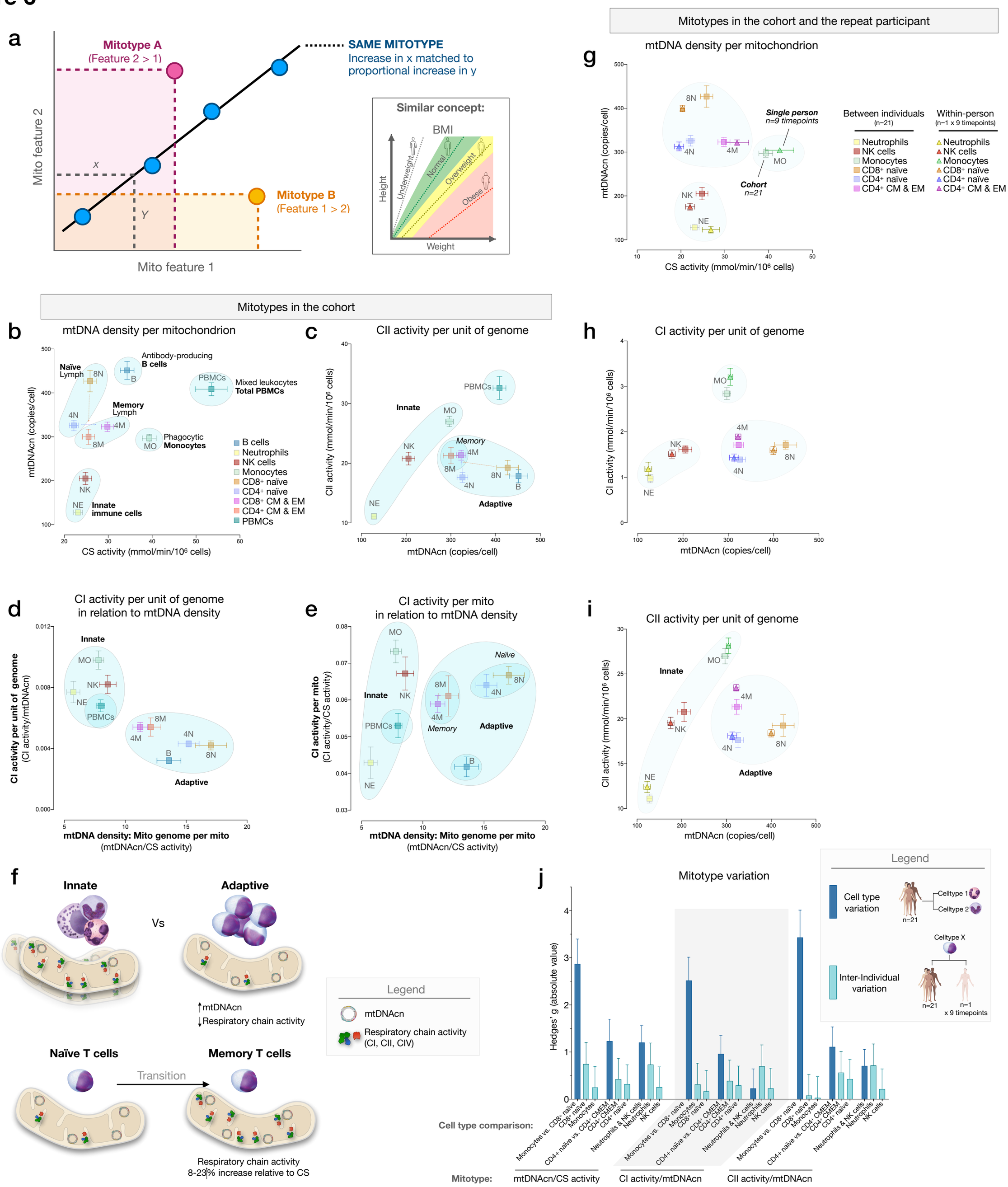

Figure 6 – Mitotypes in purified leukocyte populations from the cohort and repeated-measures.
(**a**) Schematic illustrating the multivariate approach to generate and visualize mitotypes by putting into relation two or more mitochondrial features. Notice the similarity and added insight relative to single metrics, similar to the integration of height and weight into body mass index (BMI). (**b-e**) Mitotypes plotted for each cell subtype among the cohort. Data are means and SEM. Overlaid shaded areas denote general leukocyte categories. (**f**) Summary of mitotype differences between (*i*) innate and adaptive subdivisions and (*ii*) naïve and memory T cells. (**g-i**) Validation of subtype-specific mitotype differences in the repeat participant, illustrating the conserved nature of mitotypes across individuals. Only the six cell subtypes analyzed in the repeat participant are plotted. (**j**) Comparison of the magnitude of the difference (Hedges' g) in mitotypes between cell types, and between individuals. Dark blue bars indicate the magnitude of the dominant difference in mitotypes between cell subtypes. Light blue bars indicate the magnitude of the difference in mitotypes between the cohort and the repeat participant within a cell type. Error bars reflect the 95% C.I. on the effect size.

Figure 7

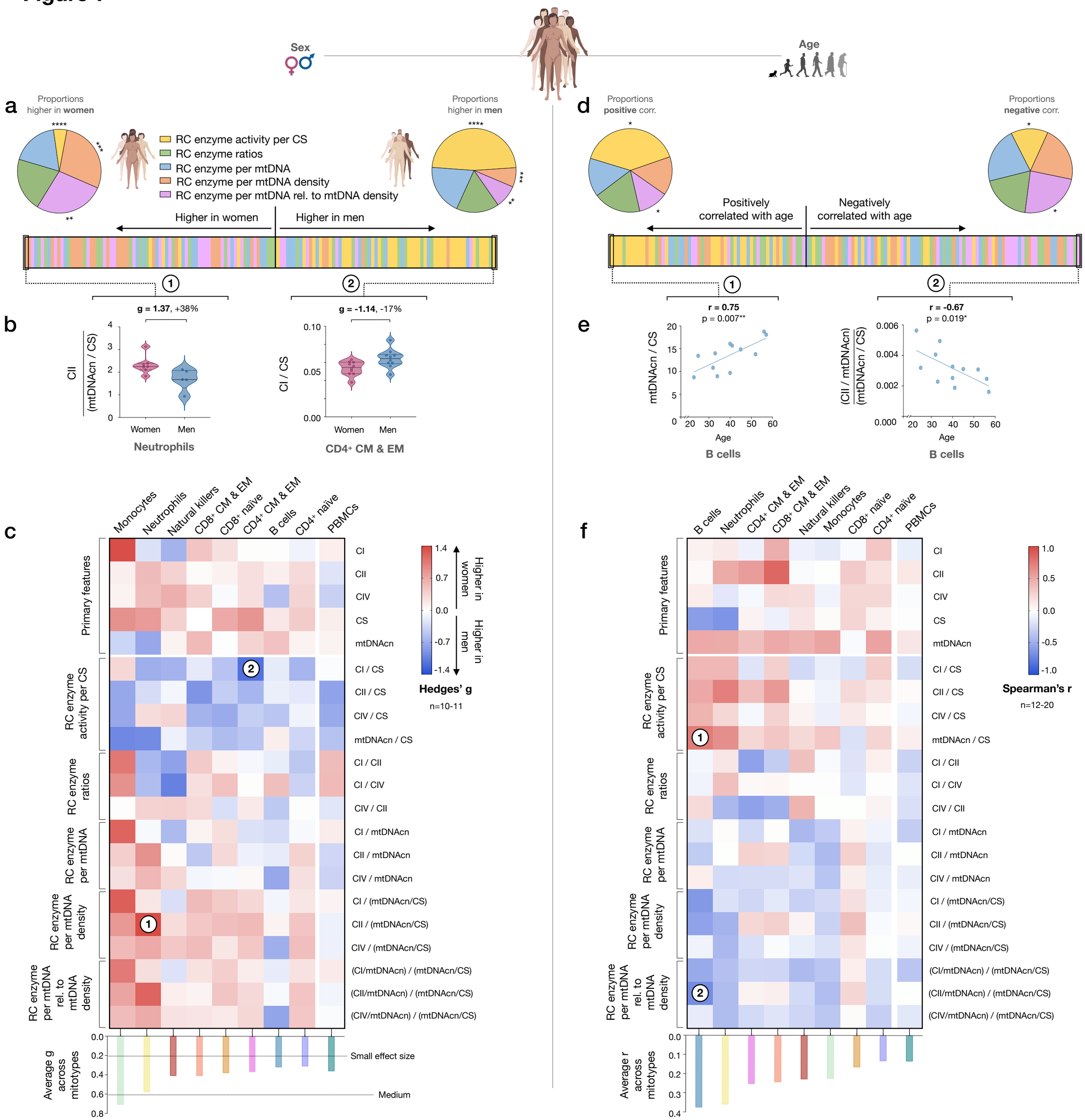

Figure 7 – Mitotype distribution and strength of difference across sex and age.

(**a**) Ranking of mitotype indices by their difference between women and men, quantified as the effect size (Hedges' g) between women and men. A total of 16 mitotype indices were generated, subdivided into 5 main color-coded categories (see Supplemental Figure 7). Pie charts illustrate the proportion mitotypes belonging to each category that are either higher in women (left) or in men (right). P-values for enrichment of sexually dimorphic mitotypes are derived from Chi-square test. (**b**) Violin plots illustrating the two mitotypes with the largest opposite sex differences, both showing large effect sizes (g). (**c**) Heatmap of sex differences (Hedges' g) for primary measures of mitochondrial function (top) and multivariate mitotypes (bottom) across cell subtypes. The histogram at the bottom shows the average absolute effect size across all mitotypes (calculated from absolute values). (**d**) Ranking of mitotype indices by the strength and direction of their association with age, with enrichment analysis analyzed as for sex (Chi-square test). (**e**) Spearman's r correlations of mitotypes/cell type combinations with the strongest positive and negative associations with age. (**f**) Heatmap of the age correlations (Spearman's r) for primary features and composite mitotypes across cell subtypes. The histogram at the bottom shows the average effect size (r) for each cell subtype (calculated using absolute values and Fisher z-transformation). p<0.05*, p<0.01**, p<0.001***, p<0.0001****.

Figure 8

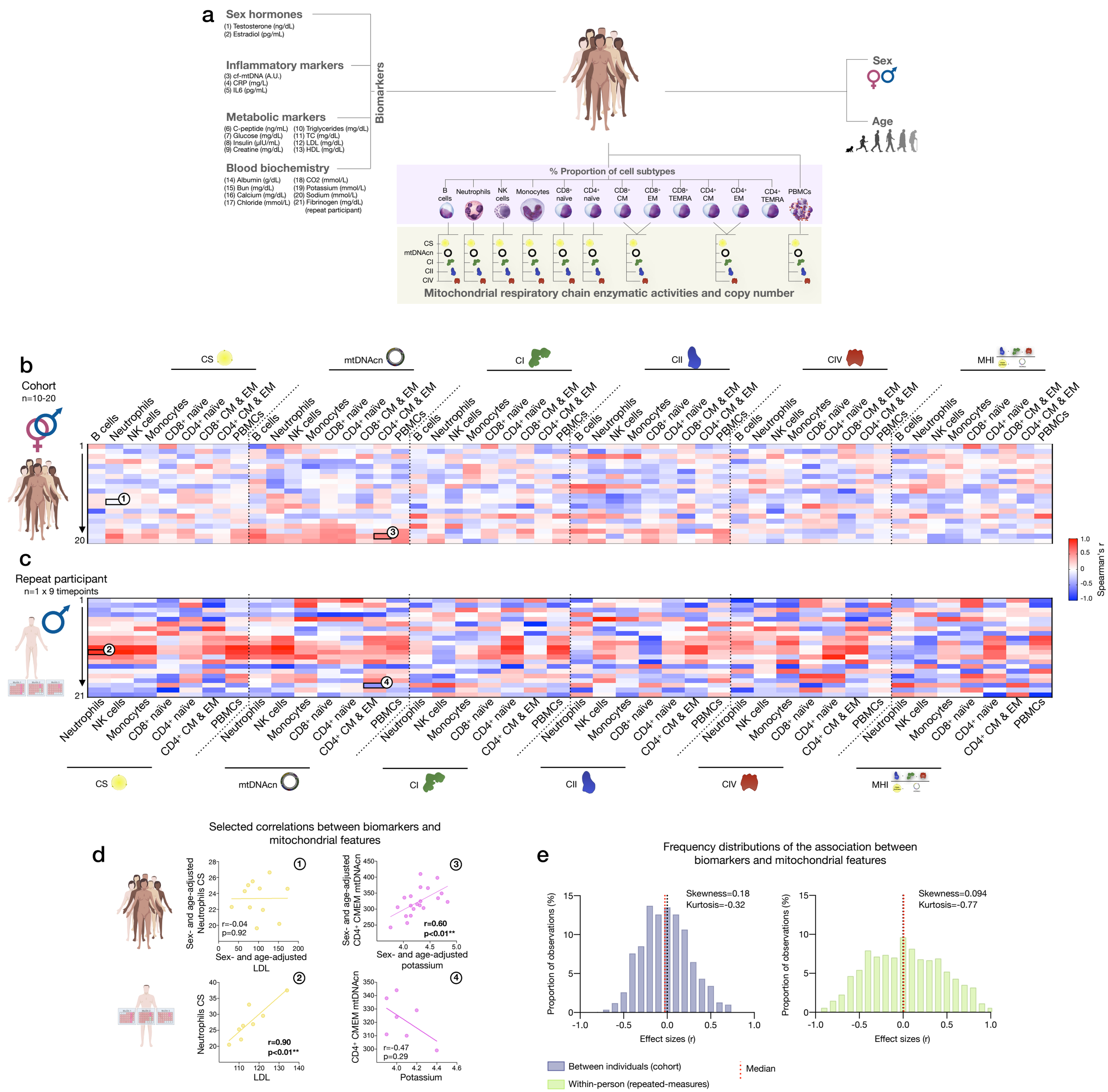

Figure 8 – Association of blood biomarkers with mitochondrial parameters across cell subtypes and primary mitochondrial features.
(**a**) Overview of blood biochemistry, hormonal, and metabolic biomarkers collected for each participant. (**b**) Sex- and age-adjusted correlations between blood biomarkers and mitochondrial features across cell subtypes for the cohort (n=10-20 per mito-biomarker combinations) shown as a heatmap. (**c**) Same as (b) but using repeated-measures of mitochondrial features and biomarkers in the repeat participant. (**d**) Scatterplots of the indicated correlations between Neutrophils CS activity and LDL cholesterol (left), and CD4+ CM-EM mtDNAcn and potassium (K^+) (right) for the cohort (top row) and the repeat participant (bottom row). (**e**) Frequency distributions of the aggregated effect sizes between biomarkers and mitochondrial features across cell subtypes for the cohort (total correlation pairs=1,080) and the repeat participant (total correlation pairs=882).

Figure 9

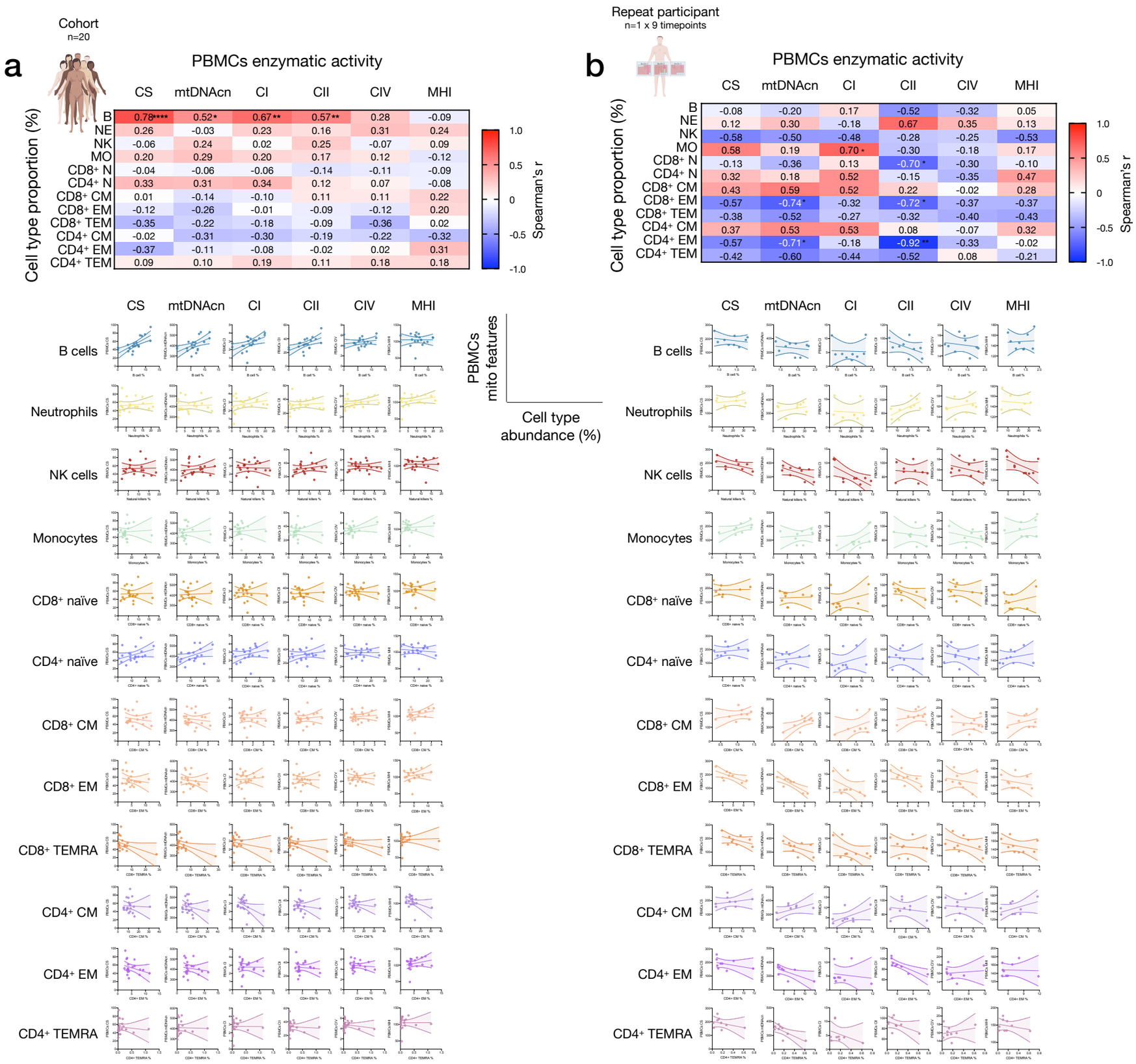

Figure 9 – Influence of cell subtypes on mitochondrial features in total PBMCs.

(**a-b**) Pairwise correlations of cell subtype proportions obtained from cell sorting with mitochondrial features measured in PBMCs for the cohort (n=20) and the repeat participant (n=1 x 9 timepoints). Aggregate correlations are shown as a heatmap (top) and individual scatterplots (bottom). (**c**) Frequency distributions of the effect sizes between PBMC mitochondrial features and cell subtypes proportions for the cohort and the repeat participant (total correlation pairs=72, for both).

Figure 10

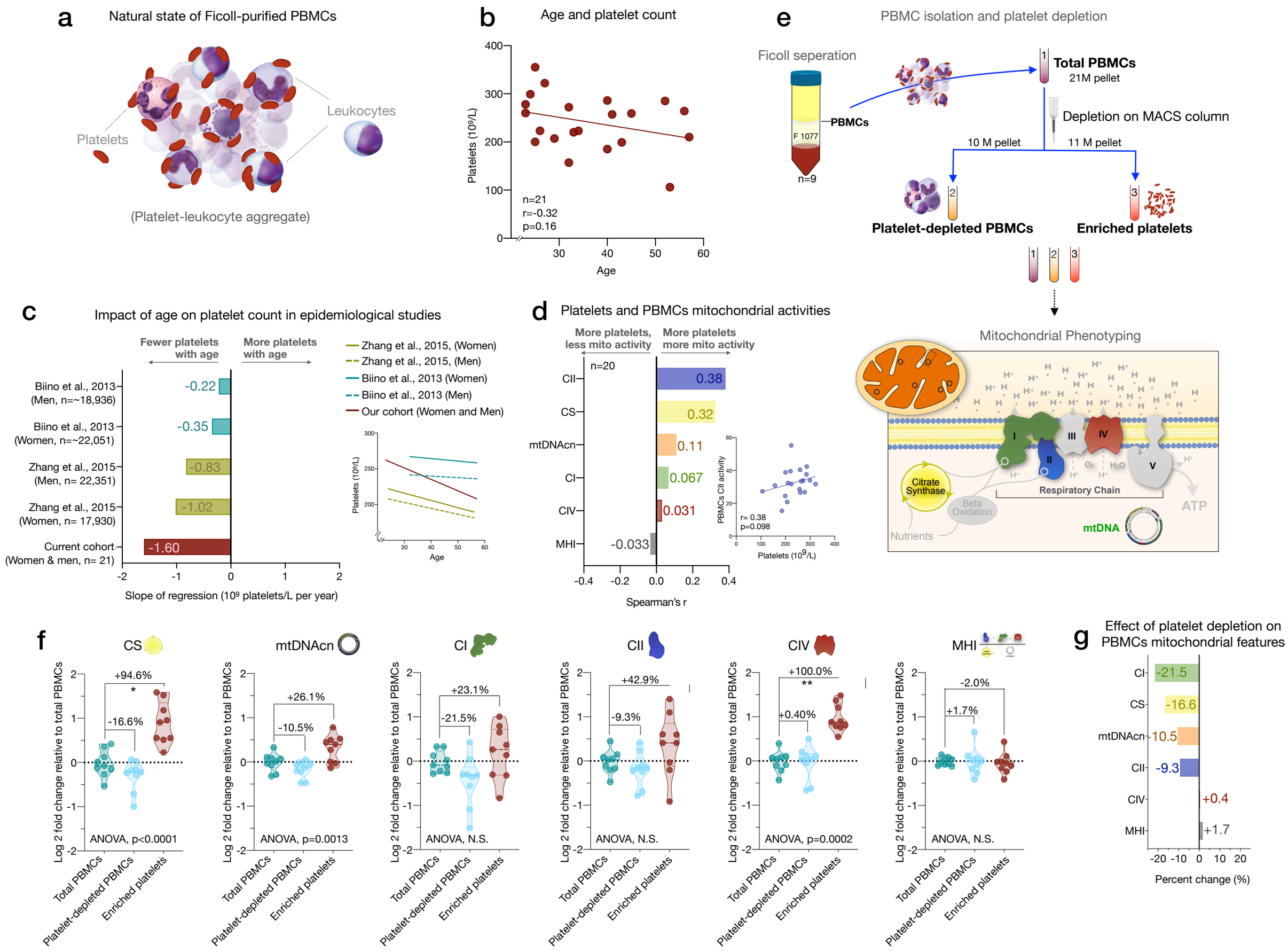

Figure 10 – Influence of platelet contamination on mitochondrial features in total PBMCs.
(**a**) Schematic of the natural state of Ficoll-isolated PBMCs associated with contaminating platelets. (**b**) Association of age and circulating platelet abundance (i.e., count) in our cohort (Spearman's r). (**c**) Change in platelet abundance as a function of age. The magnitude of the association (slope of the regression: 10^9 platelets/L per year) from two large epidemiological studies and our cohort. The inset shows the actual regressions (n=21 to 22,351). (**d**) Effect sizes of the association between platelet count and PBMCs mitochondrial features in our cohort (n=20). (**e**) Overview of the experimental PBMC platelet depletion study, yielding three different samples subjected to mitochondrial phenotyping. (**f**) Fold change in mitochondrial parameters between i) platelet-depleted PBMCs and ii) enriched platelets (with contaminating PBMCs) relative iii) total PBMCs. P-values from One-Way non-parametric ANOVA Friedman test, post-hoc Dunn's multiple comparisons relative to total PBMCs. (**g**) Percent change of platelet-depleted PBMCs mitochondrial features from total PBMCs. n=9, $p<0.05$*, $p<0.01$**, $p<0.001$***, $p<0.0001$****.